

**SUPERCritical EXTRACTION OF BINDER FROM
MULTILAYER CERAMIC CAPACITORS**

A Thesis
presented to
the Faculty of the Graduate School
at the University of Missouri-Columbia

In Partial Fulfillment
Of the Requirements for the Degree
Master of Science

by
Kumar Krishnamurthy
Dr. Stephen J. Lombardo, Thesis Supervisor

AUGUST 2008

The undersigned, appointed by the Dean of the Graduate School, have examined the thesis entitled

**SUPERCRITICAL EXTRACTION OF BINDER FROM
MULTILAYER CERAMIC CAPACITORS**

Presented by

Kumar Krishnamurthy

a candidate for the degree of

Master of Science

and hereby certify that in their opinion it is worthy of acceptance.

Dr. Stephen J. Lombardo _____

Dr. William A. Jacoby _____

Dr. Hao Li _____

ACKNOWLEDGEMENTS

I would like to take this opportunity to first thank Dr. S. J. Lombardo who has guided me and seen me through the completion of my graduate studies in University of Missouri. Of the many valuable things I have learned from him, the most important are critical thinking and critical analysis, which I intend to apply in my everyday life as well as research. Under his guidance, I have sharpened my writing, oral and analytical skills beyond my expectations and I intend to fully utilize these qualities. I would also like to thank him for the enormous patience he has shown with me throughout the course of my graduate studies and research at MU.

I would like to sincerely thank the members of my thesis committee, Dr. William Jacoby and Dr. Hao Li for giving very valuable reviews regarding my thesis and regarding the presentation of my research.

I would like to thank all my colleagues who have helped me throughout my graduate studies. I would like to first thank Dr. Jeong Woo Yun who patiently taught me all the experiments I needed to know to do research, and would always answer my questions on topics of his expertise. I would also like to thank Matt Schurwanz, Rajiv Sachanandani and Simit Patel for their help, encouragement and support. I wholeheartedly thank Rita Preckshot for all the valuable inputs she gave me for making my stay in the United States more comfortable. I sincerely thank my family back in Bombay, India whose constant support, love and encouragement helped me successfully complete my graduate studies in the United States.

TABLE OF CONTENTS

ACKNOWLEDGEMENTS	ii
LIST OF TABLES	v
LIST OF FIGURES	vi
ABSTRACT	ix
CHAPTERS	
1. GENERAL INTRODUCTION	1
1.1 STEPS IN THE FABRICATION OF A MULTILAYER CERAMIC CAPACITOR	2
1.2 SHORTCOMINGS OF THERMAL BINDER REMOVAL	4
1.3 SUPERCRITICAL EXTRACTION AS AN ALTERNATE PROCESSING STRATEGY	5
1.4 THESIS ORGANIZATION	6
1.5 REFERENCES	7
2. COMPARISON OF EFFECTS OF SUPERCRITICAL EXTRACTION ON ACRYLIC- BASED AND POLY (VINYL BUTYRAL) BASED GREEN MULTILAYER CERAMIC CAPACITORS	8
2.1 INTRODUCTION	9
2.2 EXPERIMENTAL	12
2.3 RESULTS AND DISCUSSION	15
2.4 CONCLUSIONS	29
2.5 REFERENCES	30
3. MODELING OF THE PRESSURE DISTRIBUTION IN GREEN CERAMIC BODIES DURING DEPRESSURIZATION FROM CONDITIONS OF SUPERCRITICAL EXTRACTION OF BINDER	32
3.1 INTRODUCTION	33
3.2 EXPERIMENTAL	36

3.3 MODEL.....	38
3.4 RESULTS AND DISCUSSION	41
3.5 CONCLUSIONS.....	53
3.6 REFERENCES.....	54
4. CONCLUSIONS AND FUTURE WORK.....	58
4.1 CONCLUSIONS.....	59
4.2 FUTURE WORK	61
4.3 REFERENCES.....	63
5. APPENDIX	64
A.1 INTRODUCTION.....	65
A.2 DISCRETIZATION PROCEDURE	67
A.3 MAPLE CODE FOR THE CALCULATION OF DISTRIBUTION OF PRESSURE.....	70
A.4 MATLAB CODE FOR THE CALCULATION OF DISTRIBUTION OF PRESSURE.....	72
A.5 SIMULATION RESULTS OF MAPLE AND MATLAB.....	74
A.6 REFERENCES.....	76
VITA.....	77

LIST OF TABLES

TABLE

2.1	Summary of the acrylic-based system and the PVB-based system evaluated.....	13
2.2	Summary of co-solvents used for supercritical extraction with CO ₂ at 90°C, 40 MPa for 1-h. Solute used was the G50 plasticizer (0.25 g) with a loading equal to an average amount present in an MLC.....	20
2.3	Dimensions of the acrylic-based and PVB-based MLCs used for calculating diffusivity.....	23
3.3	Summary of parameter values used for Figs. 3.3 - 3.8.....	43
A-1	Summary of values used for simulation of Figure A-2.....	75

LIST OF FIGURES

FIGURE

1.1	Steps in the fabrication of a multilayer ceramic capacitor. A thermal route for binder removal as well as a combined supercritical/thermal route are shown.....	3
2.1	Extraction vessel used for supercritical extraction of binder at 90°C and 40 MPa.....	14
2.2	Comparison of solubility of G50 plasticizer and the B72 acrylic resin with solubility of PVB and DOP for different pressures at 90-95°C.....	16
2.3	Weight loss of different organic components of the acrylic-based system versus time during supercritical extraction at 90°C and 40 MPa	17
2.4	Effect of number of 1-h cycles on weight loss of different organics of the acrylic-based system during supercritical extraction using CO ₂ at 90°C and 40 MPa.....	18
2.5	Plot of weight loss of the G50 plasticizer as a function of increasing mol % of 2-propanol in supercritical CO ₂ at 90°C and 40 MPa for a cycle time of 1-h.....	20
2.6	Effect of using 2-propanol as co-solvent with supercritical CO ₂ on the degree of binder removed from an acrylic-based and PVB-based MLCs as a function of time. Extraction conditions of 90-95°C and 40 MPa were used.....	21
2.7	Normalized extraction plotted as a function of time for the binder of the acrylic-based and PVB-based MLCs. The symbols indicate experimental values for extraction at 90°C and 40 MPa and curves indicate the calculated values of extraction for constant diffusivity.....	24
2.8	Images of an acrylic-based green MLC as received (a and b) and subjected to supercritical extraction at 90°C and 40 MPa for a cycle time of 1-h (c and d). Figures a) and c) show sides with no electrode terminations visible on the vertical faces. Figures b) and d) show electrode terminations visible on adjacent vertical faces. Weight loss of binder for c) and d) was 3.5% and depressurization was a continuous constant-temperature mode lasting ~24 h.....	26
2.9	Images of green MLCs subjected to supercritical extraction at 90°C and 40 MPa for a) single 1-h cycle and b) 11 1-h cycles. Depressurization was continuous constant temperature type, lasting ~ 24 h	27
3.1	Viscosity of carbon dioxide versus molar density at 90°C. Data are adopted from Ref. [23] and the regression curve is indicated by the solid line.....	40

3.2	Images of Sample A (above) after depressurization over 24 h and Sample B (below) after depressurization over 6 h from conditions of supercritical extraction in carbon dioxide at 90°C and 40 MPa for 1 h.....	42
3.3	Pressure of CO ₂ at 90°C versus position in the green body as a function of time for $\kappa=10^{-18}$ m ² and $\varepsilon_v=0.10$. The left-hand side corresponds to a depressurization time of $t^{DP}=0.2$ h, and the right-hand side corresponds to a depressurization time of $t^{DP}=6$ h.....	43
3.4	Behavior of $P_{n,x}$ of CO ₂ at 90°C versus position in the green body as a function of time for $\kappa=10^{-18}$ m ² and $\varepsilon_v=0.10$. The left-hand side corresponds to a depressurization time of $t^{DP}=0.2$ h, and the right-hand side corresponds to a depressurization time of $t^{DP}=6$ h.....	45
3.5	Pressure of CO ₂ at 90°C versus position in the green body as a function of time for $\kappa=10^{-16}$ m ² and $\varepsilon_v=0.15$. The left-hand side corresponds to a depressurization time of $t^{DP}=0.2$ h, and the right-hand side corresponds to a depressurization time of $t^{DP}=6$ h.....	46
3.6	Behavior of $P_{n,x}$ of CO ₂ at 90°C versus position in the green body as a function of time for $\kappa=10^{-16}$ m ² and $\varepsilon_v=0.15$. The left-hand side corresponds to a depressurization time of $t^{DP}=0.2$ h and the right-hand side corresponds to a depressurization time of $t^{DP}=6$ h.....	47
3.7	Effect of permeability on the pressure of CO ₂ at 90°C versus position in the green body for linear depressurization of $t^{DP}=0.2$ h at $t=0.1$ h (left-hand side) and for $t=0.2$ h (right-hand side).....	48
3.8	Effect of sample length scale on the pressure of CO ₂ at 90°C versus dimensionless position in the green body for linear depressurization of $t^{DP}=0.2$ h at $t=0.1$ h (left-hand side) and for $t=0.2$ h (right-hand side).....	49
3.9	Behavior of $P_{x=0}$ of CO ₂ at 90°C versus time for linear depressurization of $t^{DP}=0.2$ h for different values of γ	50
3.10	Behavior of $P_{n,x=0}$ of CO ₂ at 90°C versus time for linear depressurization of $t^{DP}=0.2$ h for different values of γ	50
A-1	Schematic representation of a discretized problem with initial value (empty circles) and boundary values (filled circles) specified. The solution is divided into a two dimensional grid with axes x and t . The grid spacing of x is h and the grid spacing of t is τ	69

A-2	Distribution of pressure in the green body during depressurization lasting a) 0.2 h (12 min) and b) 6 seconds, from conditions of 90°C and 40 MPa. The symbols indicate simulation values of Maple and lines indicate simulation values of Matlab.....	74
------------	--	----

SUPERCritical EXTRACTION OF BINDER FROM MULTILAYER CERAMIC CAPACITORS

Kumar Krishnamurthy

Dr. Stephen J. Lombardo

Thesis Supervisor

ABSTRACT

Supercritical extraction using carbon dioxide was carried out in a semi-continuous mode on the binder and its components of an acrylate-based system, the results of which were compared with a poly (vinyl butyral)-based system. To investigate the contribution of each of the binder components to overall weight loss of the acrylic-based binder, pure components as well as combination of different components were subjected to supercritical extraction.

To enhance the extraction of binder, co-solvents were evaluated on the most extractable binder component and an optimal co-solvent loading was determined. Supercritical extraction experiments were then carried out and the effect of the co-solvent on the extraction profiles was examined. To interpret the dynamics of supercritical extraction, diffusivities of the binder components of the acrylic-based and the poly (vinyl butyral based) multilayer ceramic capacitors were calculated, and were found to be in the same order of magnitude. Finally, visual analysis was performed on the acrylic-based system to suggest a mechanism that led to the formation of defects in these green ceramic bodies after the extraction process.

Supercritical extraction with carbon dioxide at 10-40 MPa and 55-90°C was used to remove binder from green multilayer ceramic bodies. Defects such as cracking and

delamination were occasionally observed in some green bodies following the extraction process, and these defects were attributed to pressure gradients that arise during depressurization from conditions of supercritical extraction. A model based on flow in porous media was thus developed to describe the temporal and spatial distribution of pressure within the green body during depressurization. The model incorporated the Peng-Robinson cubic equation of state to describe the pressure-volume-temperature behavior of the supercritical carbon dioxide, and the effect of changes in the viscosity of the supercritical fluid. The effects of the body size and gas-phase permeability on the pressure within the green body were examined.

CHAPTER 1

GENERAL INTRODUCTION

Thermal methods have been historically used to remove binder from green ceramic components. Over the years, several factors associated with the changes in the physical characteristics of the green ceramic components has resulted in these thermal methods to become a time consuming as well as an expensive process. Alternate routes to remove binder quickly and feasibly have hence become topics of interest in recent years. This thesis presents the investigations on a potentially viable technique for binder removal, i.e., the supercritical extraction of binder, which can quickly remove large fractions of binder from green ceramic components.

1.1 STEPS IN THE FABRICATION OF A MULTILAYER CERAMIC CAPACITOR

In the fabrication of multilayer ceramic capacitors (MLCs), mixtures of organic phases are used to aid in the casting and laminating of the green ceramic tapes [1]. Typically, the organic blends consist of a high molecular weight resin and a lower molecular weight plasticizer. The formulation of these organic blends is highly specialized and depends largely on the degree of particle dispersion, slurry rheology, tape flexibility, and on the tape lamination.

In industry, the fabrication of MLCs is achieved in several steps, which are illustrated in Figure 1.1. The tapes are cast using a slurry that is made by mixing the dielectric powder, binder, solvent and a dispersant in appropriate amounts. The tapes next are dried and electrodes are then screen-printed on the cut tapes, following which is the lamination step. After lamination, a green ceramic body called a green MLC is obtained

which is loaded with binder. This green MLC has to be subjected to a binder removal step prior to sintering.

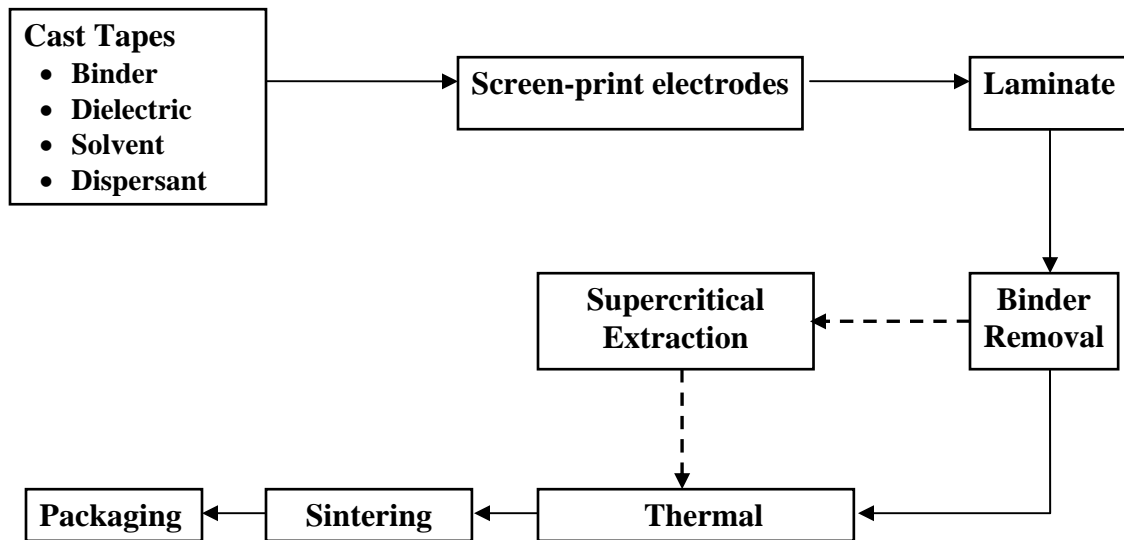


Figure 1.1: Steps in the fabrication of a multilayer ceramic capacitor. A thermal route for binder removal as well as a combined supercritical/thermal route are shown.

1.2 SHORTCOMINGS OF THERMAL BINDER REMOVAL

Different thermal methods [2] have been historically used in industry to remove binder, depending on the type of green ceramic body being processed. For example, for green MLCs with precious metal electrodes, oxidation has been employed whereas for base-metal electrodes, pyrolysis in an inert atmosphere has been the usual procedure for binder removal. Thermal binder removal degrades the binder into gas-phase products which flow out of the porous green ceramic sample, and depending on the gas-phase permeability, lead to a buildup of internal pressure. When the internal pressure buildup is high, defects such as bubbles, cracks, or fracture may occur. This has been a major shortcoming of the thermal binder removal process. In some cases, the thermal binder removal step has led to carbon residue after binder burnout, which has ultimately affected the sintered product.

Increased capacitor sizes have lead to a concomitant increase in the likelihood of internal pressure buildup in the green ceramic bodies. The use of nano-sized dielectric powders and large binder loadings has also reduced the sample permeability in the green state. All these factors have led to the use of long heating cycles for binder removal in industry to prevent damage of the ceramic body and to maintain a high yield. Long heating cycles are not only time consuming, but also costly. The thermal method of binder removal therefore has several shortcomings. Alternate routes to quickly remove binder from green MLCs and also maintain high yield have hence become recent topics of major interest.

1.3 SUPERCRITICAL EXTRACTION AS AN ALTERNATE PROCESSING STRATEGY

Supercritical extraction with carbon dioxide as the supercritical fluid has been used successfully on many green ceramic bodies [3-5]. These include injection molded and extrusion molded ceramics. More importantly, supercritical extraction has been successful in leaching up to half the initial binder loading from poly (vinyl butyral) (PVB)-based MLCs [6-8] in just a few hours; a fraction of the time as compared to the regular thermal route. The binder not extracted under supercritical conditions was then thermally removed, although this step was very rapid because of increased pore space available for the degradation products to flow out of the body easily and thus effectively mitigate pressure buildup. To this extent, supercritical extraction and a subsequent thermal cycle, as shown in Figure 1.1 (dashed line), has been successful on MLCs.

The successful implementation of supercritical extraction on PVB-based MLCs has invoked interest as to whether this technique could be used successfully on MLCs fabricated with a different binder system. For this reason, an acrylic-based binder system was evaluated in this work. No supercritical extraction results on these binder systems have been reported. This thesis therefore focuses on the results of supercritical extraction on the acrylic-based binder system and the corresponding MLCs containing this binder.

1.4 THESIS ORGANIZATION

Chapter 2 reports on the supercritical extraction results using carbon dioxide for the acrylic-based binder system and compares these to the previously reported extraction data for a PVB-based system. The solubility of the binder components from both binder systems is reported. The effect of co-solvents on weight loss of the binder in both systems is compared to weight loss profiles in the absence of a co-solvent. The dynamics of supercritical extraction for both systems are compared by calculating the diffusivities of the extractable binder components at the same operating conditions. Finally, to address the issue of defect formation in the acrylic-based MLC, visual analysis is performed on samples after supercritical extraction and a mechanism for defect formation is suggested.

To quantify the issues related to sample yield during the process of supercritical extraction, Chapter 3 presents the development of a mathematical model based on flow in porous media that is capable of calculating the spatial and temporal distribution of pressure within the green ceramic body. Chapter 3 therefore mathematically explains the method of defect formation. The model accounts for changes in viscosity of the supercritical fluid due to operating with large pressure gradients during the depressurization step. Also, the non-ideality of the supercritical fluid is taken into account. Images of the acrylic-based sample which failed, and the PVB-based sample which survived supercritical extraction at the same set of conditions, are presented. To quantify these results, simulations are performed with parameters that closely match the experimental conditions. Finally, the general effects of the body size and gas-phase permeability on the pressure within the green body are reported.

1.5 REFERENCES

1. R.E. Mistler, D.J. Shanefield, R.B. Runk, in: G. Onoda, L. Hench (Eds.), *Ceramic Processing Before Firing*, Wiley, New York, 1978.
2. R.C. Buchannan, *Ceramic Materials for Electronics: Processing Properties and Application*, Marcel Dekker Inc, New York and Basel, 1986.
3. E. Nishikawa, N. Wakao and N. Nakashima, "Binder Removal from Ceramic Green Body in the Environment of Supercritical Carbon Dioxide with and without Entrainers," *J. Supercrit. Fluids*, **4** 265-269 (1991).
4. T. Chartier, M. Ferrato and J. F. Baumard, "Supercritical Debinding of Injection Molded Ceramics," *J. Am. Ceram. Soc.*, **78** [7] 1787-92 (1995).
5. T. Chartier, E. Delhomme and J. Baumard, "Mechanisms of Binder Removal Involved of Injection Molded Ceramics," *J. De Physique III*, **7** [2], 291-02 (1997).
6. R. V. Shende, D. S. Krueger and S. J. Lombardo, "Supercritical Extraction of Binder Containing Poly(vinyl butyral) and Dioctyl Phthalate from Barium Titanate-Platinum Multilayer Ceramic Capacitors," *J. Mater. Sci.: Mater. Electron.*, **12** 637-643 (2001).
7. R. V. Shende and S. J. Lombardo, "Supercritical Extraction with Carbon Dioxide and Ethylene of Poly(vinyl butyral) and Dioctyl Phthalate from Multilayer Ceramic Capacitors," *J. Supercrit. Fluids*, **23** 153-162 (2002).
8. R. V. Shende, M. Kline and S. J. Lombardo, "Effects of supercritical extraction on the plasticization of poly(vinyl butyral) and dioctyl phthalate films," *J. Supercrit. Fluids*, **28** 113-120 (2004).

CHAPTER 2

COMPARISON OF EFFECTS OF SUPERCRITICAL EXTRACTION ON ACRYLIC - BASED AND POLY (VINYL BUTYRAL) -BASED GREEN MULTILAYER CERAMIC CAPACITORS

2.1 INTRODUCTION

The fabrication of ceramic components involves the use of blends of organic binders and plasticizers to aid in forming and handling of the green bodies. These organic blends have to be removed before the ceramic bodies can be sintered. Thermal methods [1] have been historically used in industry to remove the organic blends from the green ceramics. These methods are either oxidation or pyrolysis in an inert atmosphere depending on the type of green ceramic and its electrode. In recent years, the processing of large capacitors and the use of nano-sized powders has increased the likelihood of formation of defects because of the issue of internal pressure buildup within the ceramic sample during binder burnout. To circumvent this problem and obtain defect-free samples, industry has had to use long heating schedules that may take days to complete. Thermal methods of binder removal have therefore become time consuming and a costly procedure. Alternate methods to remove binder from the green ceramics quickly, and, in parallel, to eliminate defects, are thus topics of major interest.

In recent years, supercritical extraction has been successfully performed on injection and extrusion molded ceramics [2-8]. This technique has been used to extract a large fraction of binder from the green ceramic bodies without causing defects and in a fraction of the time as compared to the time taken by thermal routes. The binder not extracted under supercritical conditions can then be very quickly removed thermally because of the available pore space and hence effective mitigation of pressure buildup in the green body. To this extent, supercritical extraction followed by a subsequent thermal binder removal step has been shown to be a viable potential processing strategy for green ceramic components.

Supercritical extraction using CO₂ has been performed successfully on multilayer ceramic capacitors (MLCs) that have poly (vinyl butyral) (PVB) and dioctyl phthalate (DOP) as resin and plasticizer, respectively [9-13]. It was observed in these samples that about half the binder (mostly the plasticizer) could be removed in 3 h. The electrical properties measured on the samples processed via the supercritical route followed by a thermal route were similar to those measured on the samples processed solely via the thermal route [9]. It was also reported that defect-free samples could be obtained by minimizing the pressure gradient and by preventing formation of dry ice during depressurization.

Since supercritical extraction at 95°C and 40 MPa was a success for the PVB-based system [9-13], it was of prime interest to investigate if supercritical extraction could be performed with the same success rate on an acrylic-based system, the results for which have not been reported. This chapter is hence focused on the results of supercritical extraction at 90°C and 40 MPa on acrylic-based MLCs and compares the results with those of the PVB-based system, the data for which are adopted from Ref. [9].

The binder blend for the acrylic-system consists of a B72 acrylic resin and a G50 polyester adipate. Supercritical extraction is performed on the acrylic-based binder in the MLC as well as on the individual binder components to understand the contribution of each component to the overall weight loss. To enhance extraction at 90°C and 40 MPa, various co-solvents (or entrainers) are evaluated, and optimization of the most effective co-solvent is performed on the most extractable binder component. To compare the dynamics of supercritical extraction of binder from the acrylic-based and the PVB-based MLCs, the diffusivities of the extractable binder components are compared at operating

conditions of 90-95°C and 40 MPa. Finally, a thorough visual analysis for the occurrence of defects is performed on the acrylic-based samples and a mechanism for their formation is suggested.

2.2 EXPERIMENTAL

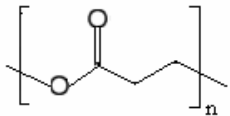
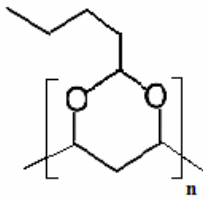
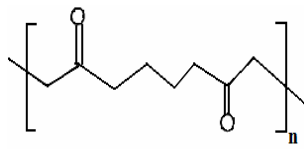
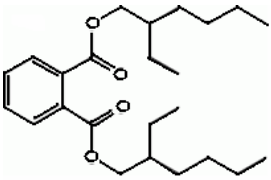
The acrylic-based system is comprised of green tapes made from LN 0F61 N2200 BaTiO₃-based ceramic powder and a WC101 binder mixture (Wright Capacitors, Inc., Santa Ana, CA). The binder mixture was 31.5 wt.% B72 acrylic resin, 6.1 wt.% G50 adipate plasticizer and 62.4 wt.% methyl ethyl ketone (MEK). The individual green tapes were 0.01 inch thick and were laminated into MLCs that had 41 active layers. The electrode used in the MLCs was of a precious metal. The dimensions of the acrylic-based MLC after lamination were $2.1 \times 2 \times 1$ cm ($0.86 \times 0.78 \times 0.41$ inch) when in the green state. In this investigation, the acrylic-based system described above was compared to a PVB-based system, details for which are given elsewhere [9-13]. Table 2.1 highlights the main attributes of both the binder systems.

Figure 2.1 shows an illustration of the extraction vessel used for all the experiments in this investigation. The vessel used was a SS316 (6.25 cm diameter, 500 ml) Parr high pressure non-stirred type which was placed in a controlled temperature bath for temperatures up to 90°C. The vessel was equipped with a thermocouple and a pressure gauge for maintaining the temperature and pressure within $\pm 5^\circ\text{C}$ and ± 1 MPa respectively. The supercritical fluid used was carbon dioxide.

The extraction experiments were conducted in a semi-continuous mode and the extent of binder (organic) removal was determined by measuring weight loss of the sample and normalizing it to the amount of binder initially present. The samples related to the acrylic-based system were exposed from 1 to 11 cycles of supercritical fluid. Each cycle was comprised of a pressurization step, a dwelling step and a depressurization step. The pressurization step would start from 0.1 MPa and typically last a few minutes until

reaching the extraction pressure. The dwelling step was for 1 hour (thus named a 1-h cycle) during which the pressure in the vessel was constant. The dwelling step was followed by a depressurization step, which was carried out at constant-temperature, lasting ~ 24 h.

Table 2.1: Summary of the acrylic-based system and the PVB-based system evaluated.

	Component (Weight %)	Component (Weight %)
Dielectric	BaTiO ₃ -based (88.1)	BaTiO ₃ (90)
Resin and structural unit	B72 acrylate (9.9) 	Poly (vinyl butyral) (5.5) 
Plasticizer and structural unit	G50 polyester adipate (2.0) 	Diethyl phthalate (4.5) 

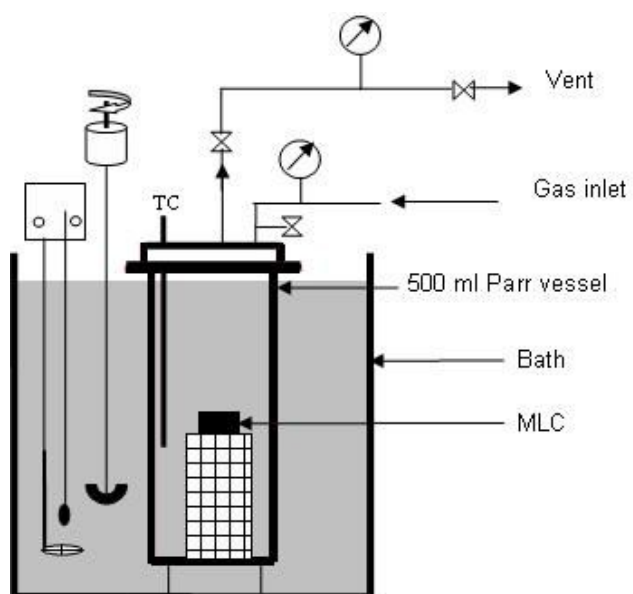


Figure 2.1: Extraction vessel used for supercritical extraction of binder at 90°C and 40 MPa.

2.3 RESULTS AND DISCUSSION

Extraction experiments

The extent of supercritical extraction of binder from ceramic bodies depends largely on the solubility of the binder components in the supercritical fluid at a given temperature and pressure. A binder component with high solubility in a supercritical fluid may undergo a large degree of extraction, and, depending on its weight % loading in the green ceramic, may generate more open pore space.

It was previously established that the weight loss of the organic components increased with increasing temperature and pressure [9]. Solubility of the organic components is therefore reported at 90-95°C in Figure 2.2, which shows that solubility of the organic components for both binder-systems increases with increasing pressure at a fixed temperature, and hence, with increasing density of CO₂. More importantly, the solubility of the extractable component of the plasticizers is more by an order of magnitude as compared to the solubility of the resins.

For the acrylic-based system, supercritical extraction was performed on the individual organic components at 90°C and 40 MPa to investigate their contribution to the weight loss of binder. Figure 2.3 shows that as the number of cycles increases more binder is extracted until the curves plateau close to 11 1-h cycles. Supercritical extraction on the pure G50 plasticizer yielded a total weight loss of 34% whereas the total weight loss for the pure B72 resin was ~0%. The behavior of the plasticizer being more extractable than the resin is consistent with results reported for the poly (vinyl butyral)-DOP polymer blend [9] and poly (vinyl chloride)-DOP polymer blend [14]. The

maximum amount of binder extracted from the MLC is 10.45% and also exhibits a plateau in extraction behavior after 11 1-h cycles.

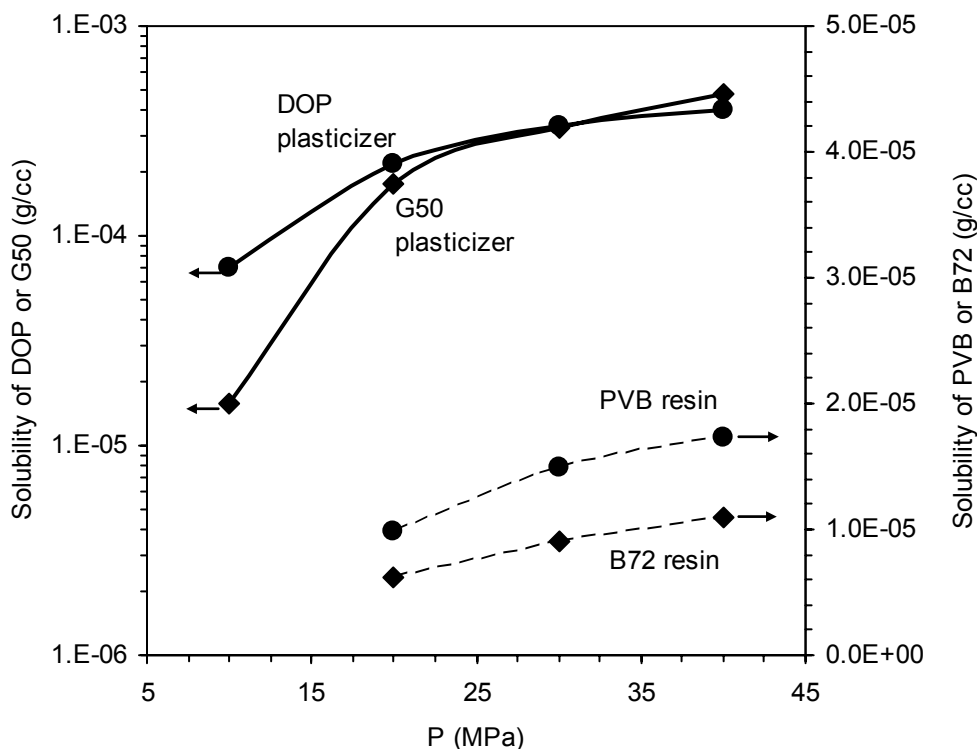


Figure 2.2: Comparison of solubility of G50 plasticizer and the B72 acrylic resin with solubility of PVB and DOP for different pressures at 90-95°C.

The extraction results in Figure 2.3 suggest that the G50 plasticizer (a polyester adipate) is not a pure material. If it were, then repeated exposure to fresh charges of CO₂ would lead to additional extraction, and in principle should lead to 100% extraction after sufficient number of charges. The plateau in the extraction behavior of the G50 plasticizer suggests that about 2/3rd of the pure G50 is not soluble. Such behavior may arise because of either a distribution of molecular weights or due to different components within the G50. This behavior then also translates into a plateau in the extraction behavior from the MLCs.

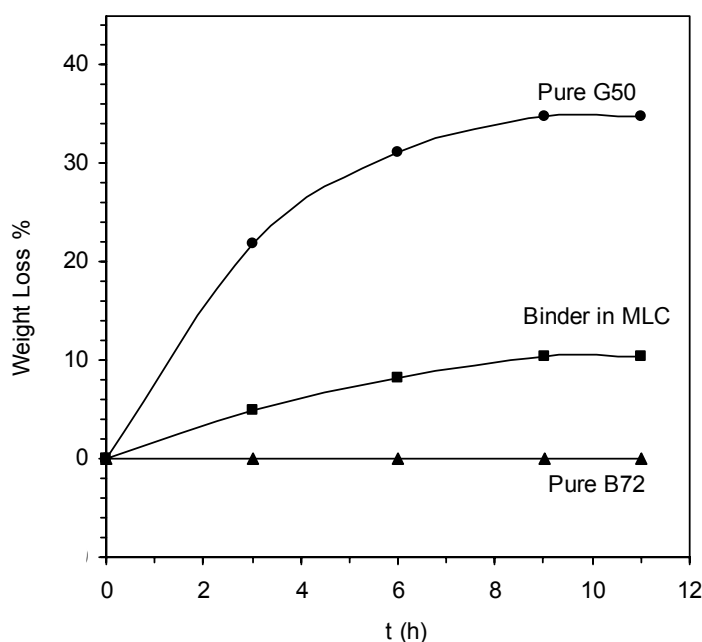


Figure 2.3: Weight loss of different organic components of the acrylic-based system versus time during supercritical extraction at 90°C and 40 MPa.

Based on the composition in Table 2.1, full extraction of the G50 would lead to a 16% weight loss of binder in the MLC. For the G50 alone, however, the results in Figure 2.3 show that only about one-third of the G50 is soluble, which should then translate into ~5% extraction of binder. We see, however, that in fact about twice this amount is achieved; such behavior may arise from interactions between the two components in the binder blend.

To test this idea, samples of both G50 and the B72 (denoted as G50/B72) were present in the extraction vessel simultaneously in separate containers, and thus had no direct contact with each other except through the supercritical phase. The weights of the G50 (~0.25 g) and the B72 (~1.25 g) used were approximately equal to the average weights as would be present in an as-received MLC. The results in Figure 2.4 show that when experiments are conducted in this fashion, enhanced solubility of each component

is observed as compared to when the organic components are alone in the vessel. Such behavior may arise because of mutual plasticization of the two components on each other, through the supercritical phase, which allows the molecules to be more easily separated from each other.

The G50 lost 40% of its weight when present as the G50/B72, as compared to 34% weight loss when present alone in the vessel. The B72 lost 1.2% of its weight when present as the G50/B72, as opposed to its negligible weight loss when present alone. This suggested that more contribution to weight loss of binder for the acrylic-based MLCs was from G50, although B72 may have also contributed to its overall weight loss. The behavior of the plasticizer dominating in its contribution to weight loss of binder from a green MLC during supercritical extraction was also observed for the PVB-based system [9].

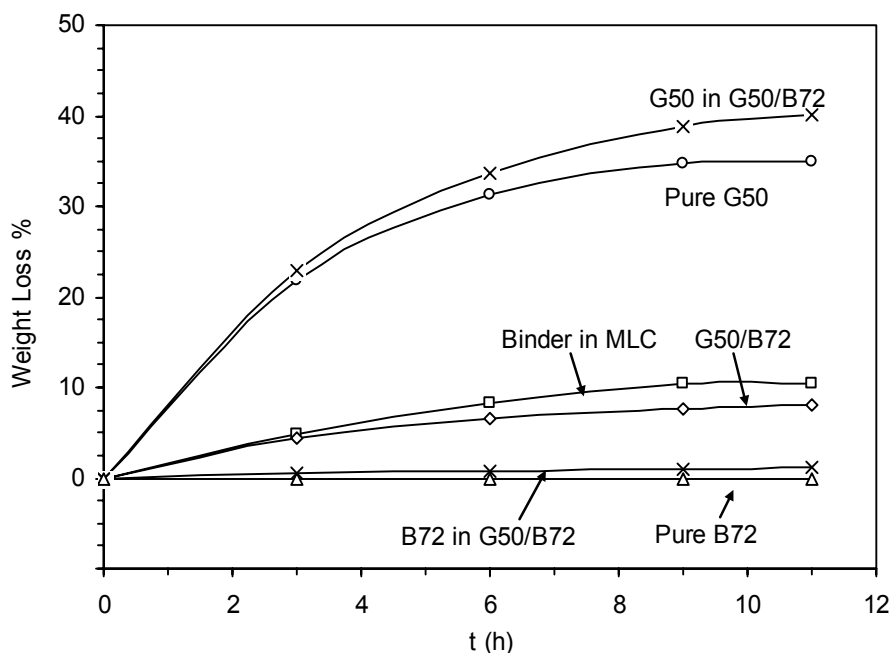


Figure 2.4: Effect of number of 1-h cycles on weight loss of different organics of the acrylic-based system during supercritical extraction using CO₂ at 90°C and 40 MPa.

To increase the solubility of organics in supercritical fluids, a common strategy is to add small amounts of a second fluid; such fluids are called entrainers or co-solvents. Based on this idea, MLCs were exposed to supercritical extraction in CO₂ at 40 MPa and 90°C for 1-h in order to screen different co-solvents. Table 2.2 shows that for the four co-solvents evaluated, all lead to a significant enhancement by a factor of 5-15 in the weight loss of the G50. The most effective of these co-solvents is 2-propanol.

To probe in more detail the effect of the co-solvent, extraction experiments at 90°C and 40 MPa for 1-h were conducted with different amounts of 2-propanol, expressed as a mol % in terms of the CO₂ in the extraction vessel. Figure 2.5 shows that the weight loss of G50 is a strong function of the mol % of 2-propanol, with the optimum located at approximately 0.7 mol %. This optimum corresponds to an enhancement factor of 12 as compared to when no entrainer is used. Supercritical extraction results on paraffin based injection molded ceramics [15] using iso-octane as a co-solvent also observed the presence of a similar kind of optimum in the plot of weight loss versus mol % co-solvent loading. Presences of such optima were attributed to the use of branched chain organic co-solvents. It was also mentioned in Ref. [15] that as the co-solvent loading was increased to beyond the optimum, eventually there was inhibition of extraction of the paraffin binder, to values less than the case of no-entrainer loading. No such behavior was detected for the acrylic-based system.

Table 2.2: Summary of co-solvents used for supercritical extraction with CO₂ at 90°C, 40 MPa for 1-h. Solute used was the G50 plasticizer (0.25 g) with a loading equal to an average amount present in an MLC.

Co-solvent used (5 ml)	% Weight loss
None	4.1
Methanol	56.5
Ethanol	22.5
2-propanol	61.4
Water	24.9

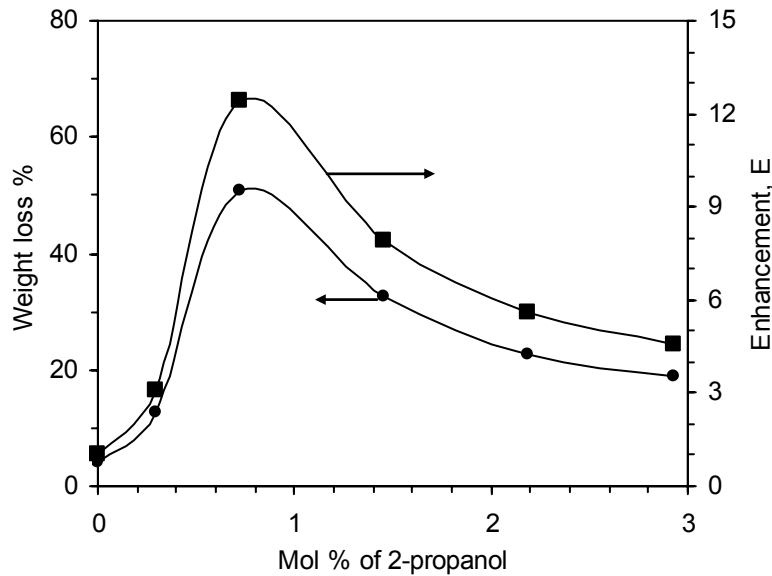


Figure 2.5: Plot of weight loss of the G50 plasticizer as a function of increasing mol % of 2-propanol in supercritical CO₂ at 90°C and 40 MPa for a cycle time of 1-h.

Based on these results, the acrylic-based MLCs were subjected to supercritical extraction with the optimum loading of 2-propanol added to the vessel before the 1st, 4th, 7th and 10th cycle. Figure 2.6 shows that the presence of the 2-propanol leads to an enhancement in the weight loss by about 20% for the binder of the acrylic-based MLC.

Based on the total mass of organic components, however, this only corresponds to a modest amount of additional organic component extracted. For the binder of PVB-based MLC the presence of 2-propanol does not enhance the overall amount of binder extracted [9].

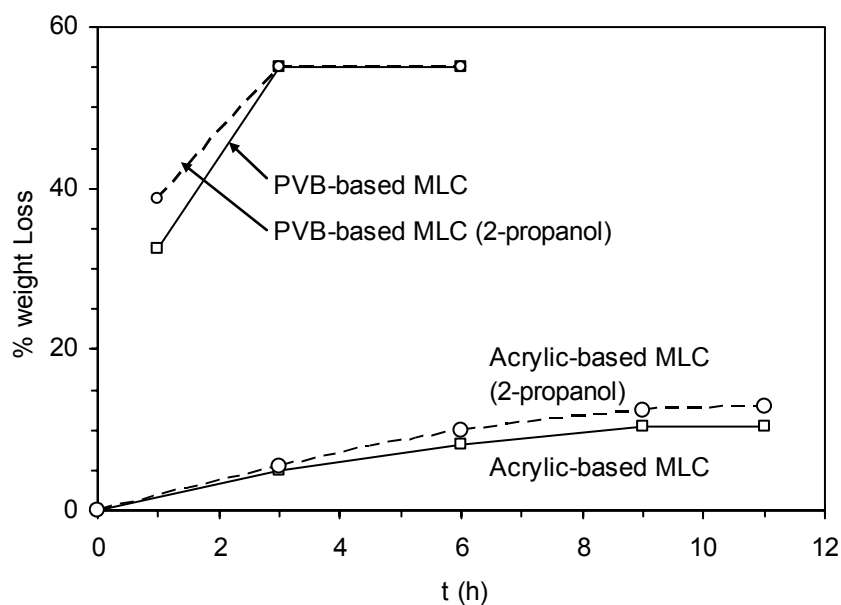


Figure 2.6: Effect of using 2-propanol as co-solvent with supercritical CO₂ on the degree of binder removed from an acrylic-based and PVB-based MLCs as a function of time. Extraction conditions of 90 - 95°C and 40 MPa were used.

Diffusion Calculation

At the start of a cycle, pressurizing the vessel forces CO₂ into the pores of the MLC. Once the CO₂ has impregnated the MLC, extraction begins at supercritical conditions ($T \geq T_c$ and $P \geq P_c$) by the dissolution of binder into the CO₂ phase followed by diffusion of the extracted binder out of the MLC [5-9]. This can be mathematically explained using an unsteady state diffusion equation, which is expressed for parallelepiped geometries with sides of lengths L_x , L_y and L_z by

$$\frac{\partial C}{\partial t} = D \left(\frac{\partial^2 C}{\partial x^2} + \frac{\partial^2 C}{\partial y^2} + \frac{\partial^2 C}{\partial z^2} \right) \quad (2.1)$$

where C is the concentration of binder in the supercritical phase and D is its diffusivity, assumed to be a constant. The initial condition is described by $C(x, y, z, 0) = C_o$ and at the boundary by $C(x, y, z, t) = 0$, with $x = \pm L_x/2$, $y = \pm L_y/2$ and $z = \pm L_z/2$. The latter condition was not precisely satisfied because of operating in a semi-continuous mode. The solution to Eq. 2.1 for the average concentration of binder with prescribed boundary conditions is [5,6,9]

$$\frac{\bar{C}}{C_o} = \frac{512}{\pi^6} \sum_{i=0}^{\infty} \sum_{j=0}^{\infty} \sum_{k=0}^{\infty} \frac{\exp(-\alpha_{ijk} t)}{[(2i+1)(2j+1)(2k+1)]^2} \quad (2.2)$$

where

$$\alpha_{ijk} = \frac{D\pi^2}{4} \left[\left(\frac{2i+1}{L_x/2} \right)^2 + \left(\frac{2j+1}{L_y/2} \right)^2 + \left(\frac{2k+1}{L_z/2} \right)^2 \right] \quad (2.3)$$

Equations 2.2 and 2.3 were thus used to calculate the diffusivity of binder in supercritical CO₂ for each of the binder systems. Table 2.3 summarizes the dimensions of the PVB-

based and acrylic-based MLCs. Data for Eqs. 2.2 and 2.3 were taken from Figure 2.6 and Table 2.3 to calculate the diffusivity of binder for each system.

Table 2.3: Dimensions of the acrylic-based and PVB-based MLCs used for calculating diffusivity.

Organic system	Dimensions (cm)		
	L_x	L_y	L_z
Acrylic-based MLC	2.1	2.0	1.0
PVB-based MLC [9]	1.5	1.4	0.25

Figure 2.7 shows the plot of normalized extraction rate as a function of time for both systems. The symbols indicate the experimental extraction data normalized with the total amount of extractable binder in each case. The curves indicate the data corresponding to the calculated diffusivity values. On comparing with the extractable binder from the PVB-based MLC which was reported to have a diffusivity value of $1 \times 10^{-10} \text{ m}^2/\text{s}$ [9], the extractable binder from the acrylic-based MLC had diffusivity value of $3.2 \times 10^{-10} \text{ m}^2/\text{s}$, which was thrice as high. A possible reason for a higher value of diffusivity for the acrylic-based system could be the defects present in the MLC throughout the extraction process, which will be presented later.

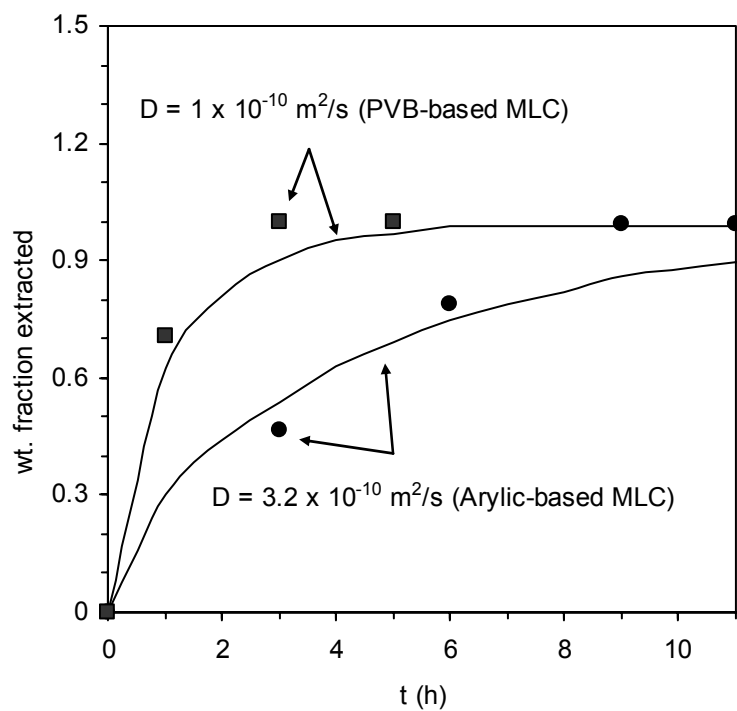


Figure 2.7: Normalized extraction plotted as a function of time for the binder of the acrylic-based and PVB-based MLCs. The symbols indicate experimental values for extraction at 90°C and 40 MPa and curves indicate the calculated values of extraction for constant diffusivity.

Defect Formation in Acrylic-based MLCs

The defects that occur in MLCs are mainly due to a pressure gradient within the ceramic body. A pressure gradient arises due to a lag time of equilibration between the pressure within the ceramic sample and the vessel during depressurization [13]. Depressurization itself can be carried out in different ways. When carried out by adiabatic throttling [13], the CO₂ in the vessel undergoes an iso-enthalpic expansion during which temperature in the vessel changes with reducing pressure. Depending upon the initial conditions in the vessel and hence, of CO₂, this iso-enthalpic expansion during depressurization may result in the formation of dry ice. An alternative to adiabatic throttling is a constant-temperature continuous depressurization. In this mode with the starting temperature over the critical temperature and constant during depressurization, the formation of dry ice is avoided when CO₂ is released from the vessel.

To address the issues related to the yield of acrylic-based MLCs, visual analysis was done to observe defect trends after depressurization. Figures 2.8a and 2.8b show the adjacent faces of an as received MLC before extraction. Figure 2.8c shows the cracks on the MLC surface without electrodes, after extraction at 90°C and 40 MPa and depressurization lasting ~24 h. These cracks are predominantly horizontal with visible vertical jumps. Figure 2.8d shows that the primary damage has occurred along the same horizontal plane as the electrode. Vertical cracks are visible around the edges and near the center. The length of some of the vertical cracks around the center is similar to the vertical distance between two electrode planes.

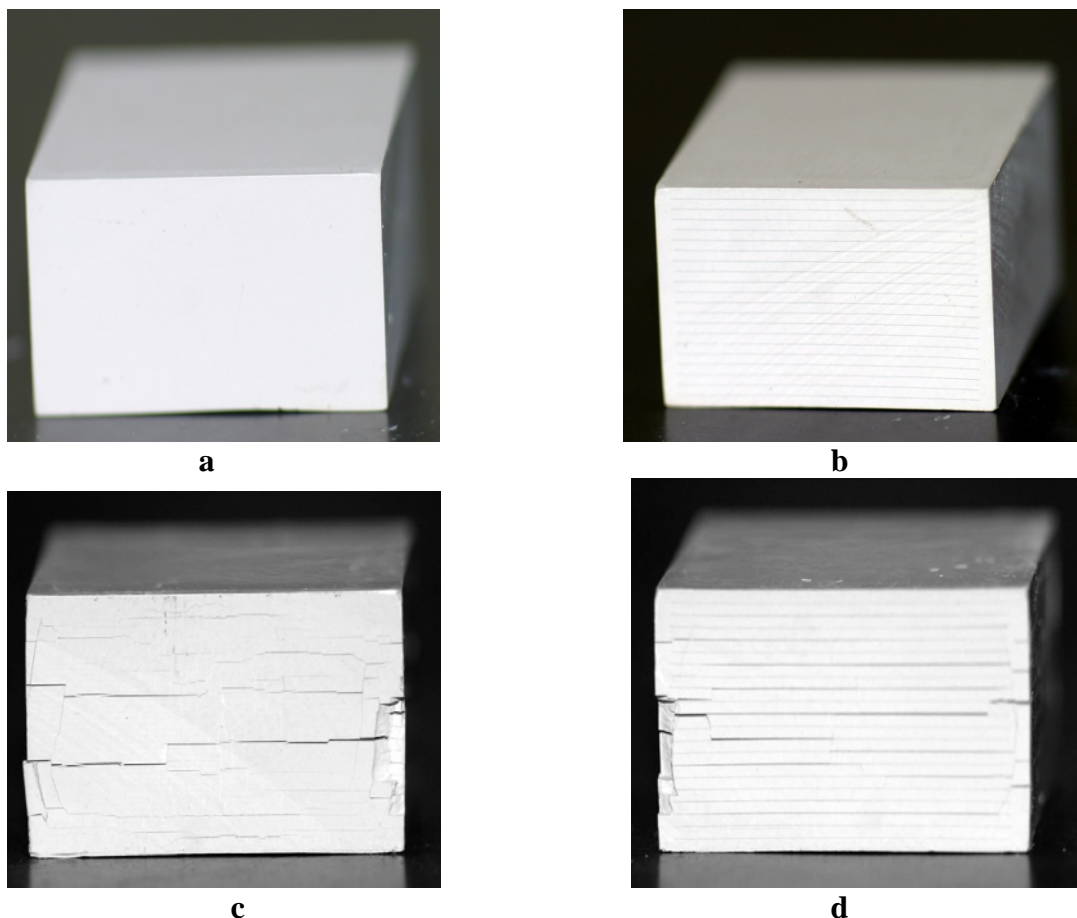


Figure 2.8: Images of an acrylic-based green MLC as received (a and b) and subjected to supercritical extraction at 90°C and 40 MPa for a cycle time of 1-h (c and d). Figures a) and c) show sides with no electrode terminations visible on the vertical faces. Figures b) and d) show electrode terminations visible on adjacent vertical faces. Weight loss of binder for c) and d) was 3.5% and depressurization was a continuous constant-temperature mode lasting ~24 h.

The samples shown in Figure 2.9 were subjected to a single 1-h and 11 1-h cycles to observe the difference in surface defects. The damage observed in Figure 2.9b is similar to the damage in Figure 2.9a. Most of the damage may have occurred after the end of the first dwell period, during the first depressurization. At the end of the first

cycle, the binder lost is less than the total amount of binder lost after 11 cycles. The permeability of the sample may have hence been insufficient at the end of the first cycle to mitigate pressure buildup during depressurization.

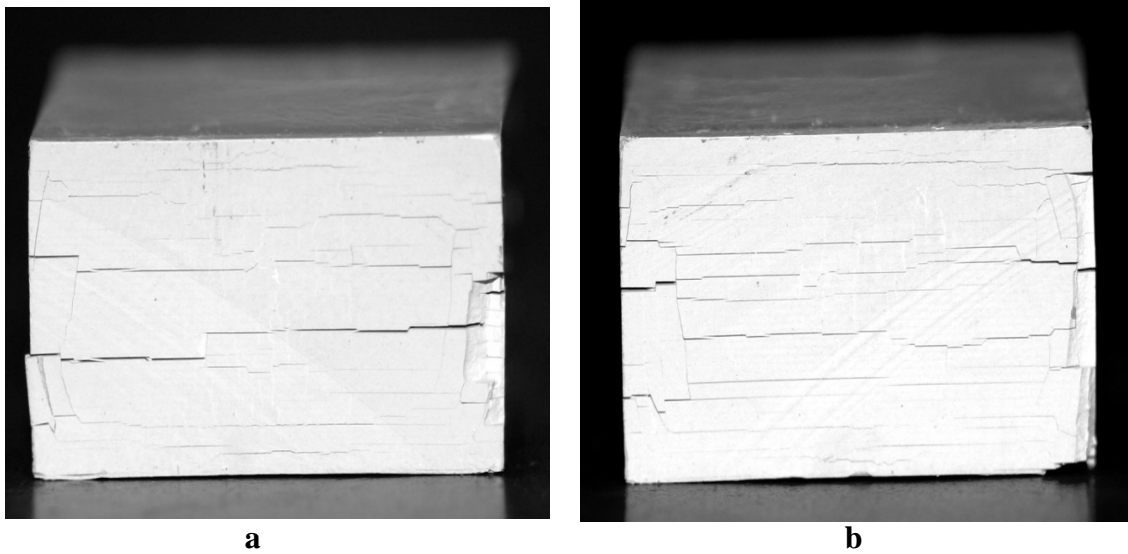


Figure 2.9: Images of green MLCs subjected to supercritical extraction at 90°C and 40 MPa for a) single 1-h cycle and b) 11 1-h cycles. Depressurization was continuous constant temperature type, lasting ~ 24 h.

In summary, for the PVB-based MLCs about 55% binder was extracted, with the process going to ~70% completion in the first cycle itself. The large amount of binder extracted (mostly DOP) therefore introduced more porosity in the MLC before depressurization started. Presence of a larger pore volume at this stage resulted in less buildup of pressure when CO₂ was flowing out of the pores of the MLC due to forced convection. The yield of the PVB-based MLCs was therefore high, and defects in them were avoidable [13].

Conversely, the acrylic-based MLCs experienced defects after the first 1-h cycle at 90°C and 40 MPa, even after depressurization lasted ~24 h. Only ~3.5 % binder was

extracted in the first cycle as opposed to the PVB-based MLC, which lost ~32% binder. The weight loss of binder for the acrylic-based MLCs was therefore small and the creation of pore volume was insignificant; this translated directly to the sample lacking permeability, hence resulting in defects. Also, the presence of these defects during extraction resulted in more surface area as compared to a defect-free sample, which may have led to higher diffusivity value of the extractable binder component.

2.4 CONCLUSIONS

Supercritical extraction using CO₂ was performed at 90°C and 40 MPa on an acrylic-binder system, the results of which were compared to previously reported data for the PVB-based system. The solubility of the corresponding resins and the plasticizers were in the same order of magnitude. Interactions existed within the binder components of the acrylic-based system. The contribution to total weight loss was therefore not purely by the plasticizer. Enhancement of extraction using 2-propanol as a co-solvent resulted in a modest increase in extraction for the binder of the acrylic-based MLCs as compared to no enhancement for binder of the PVB-based MLCs. The diffusivity of the extractable binder of the two systems was of the same order of magnitude, although, the diffusivity related to the acrylic-based MLC was thrice as high. Defects in the PVB-based MLCs were infrequent but for the acrylic-based MLCs, the defects always existed after depressurization. This was due to ineffective mitigation of pressure buildup in the latter MLC system, resulting from the lack of sample permeability.

2.5 REFERENCES

1. J.A. Lewis, "Binder Removal from Ceramics", *Ann. Rev. Mater. Sci.*, **27** 147-173 (1997).
2. D. W. Matson and R. D. Smith, "Supercritical Fluid Technologies for Ceramic-Processing Applications," *J. Am. Ceram. Soc.*, **72** [6] 871-881 (1989).
3. S. Nakajima, S. Yasuhara, and M. Ishihara, "Method of Removing Binder Material from a Shaped Ceramic Preform by Extracting with Supercritical Fluid," US Patent No. 4,731,208, March 15, 1988.
4. T. Miyashita, Y. Ueno, H. Nishio, and S. Kubodera, "Method for Removing the Dispersion Medium from a Molded Pulverulent Material," US Patent No. 4,737,332, April 12, 1988.
5. E. Nishikawa, N. Wakao and N. Nakashima, "Binder Removal from Ceramic Green Body in the Environment of Supercritical Carbon Dioxide with and without Entrainers," *J. Supercrit. Fluids*, **4** 265-269 (1991).
6. T. Chartier, M. Ferrato and J. F. Baumard, "Supercritical Debinding of Injection Molded Ceramics," *J. Am. Ceram. Soc.*, **78** [7] 1787-92 (1995).
7. T. Chartier, E. Delhomme and J. Baumard, "Mechanisms of Binder Removal Involved of Injection Molded Ceramics," *J. De Physique III*, **7** [2], 291-02 (1997).
8. T. Chartier, E. Delhomme, J. F. Baumard, P. Marteau, P. Subra and R. Tufeu, "Solubility in Supercritical Carbon Dioxide, of Paraffin Waxes Used as Binders for Low-Pressure Injection Molding," *Ind. Eng. Chem. Res.*, **38** [5] 1904-10 (1999).

9. R. V. Shende, D. S. Krueger and S. J. Lombardo, "Supercritical Extraction of Binder Containing Poly (vinyl butyral) and Dioctyl Phthalate from Barium Titanate-Platinum Multilayer Ceramic Capacitors," *J. Mater. Sci.: Mater. Electron.*, **12** 637-643 (2001).
10. R.V. Shende, D.S. Krueger and S.J. Lombardo, "Binder Removal by Supercritical Extraction from BaTiO₃-Pt Multilayer Ceramic Capacitors," accepted to Ceramic Transactions, Innovative Processing/Synthesis: Ceramics, Glasses, Composites IV, American Ceramic Society, Westerville, OH, p. 165 (2001).
11. R. V. Shende and S. J. Lombardo, "Supercritical Extraction with Carbon Dioxide and Ethylene of Poly(vinyl butyral) and Dioctyl Phthalate from Multilayer Ceramic Capacitors," *J. Supercrit. Fluids*, **23** 153-162 (2002).
12. R. V. Shende, M. Kline and S. J. Lombardo, "Effects of supercritical extraction on the plasticization of poly(vinyl butyral) and dioctyl phthalate films," *J. Supercrit. Fluids*, **28** 113-120 (2004).
13. R. V. Shende, T. R. Redfern and S. J. Lombardo, "Defect Formation during Supercritical Extraction of Binder from Green Ceramic Components," *J. Am. Ceram. Soc.*, **87** [7] 1254-1258 (2004).
14. M.L. Martin, A. Jimenez, V. Berenguer and J. Lopez, "Optimization of Variables on the Supercritical Fluid Extraction of Phthalate Plasticizers," *J. Supercrit. Fluids*, **12** [3] 271-277 (1998).
15. F. Bordet, T. Chartier, J. F. Baumard, "The Use of Co-Solvents in Supercritical Debinding of Ceramics," *J. European Ceram. Soc.*, **22** 1067-1072 (2002).

CHAPTER 3

**MODELING OF THE PRESSURE DISTRIBUTION IN GREEN
CERAMIC BODIES DURING DEPRESSURIZATION FROM
CONDITIONS OF SUPERCRITICAL EXTRACTION OF BINDER**

3.1 INTRODUCTION

The supercritical extraction of organic binders from green ceramic components has been examined over the last few decades by a number of researchers [1-12]. Such a processing approach may offer a number of advantages as compared to more conventional thermal removal of binder. For example, supercritical extraction with carbon dioxide may be used to remove large fractions of binder in periods of times as short as a few hours, as compared to the 10-100's of hours for the thermal removal of binder from highly loaded samples. Supercritical extraction has been shown to be especially effective in removing organic components of low molecular weight, but less so for higher molecular weight species. The addition of a co-solvent or entrainer may also be used to enhance further the removal of organics species from green ceramic bodies. Even though in some cases supercritical extraction cannot remove all of the organic species, the subsequent thermal removal of the remaining binder may be greatly accelerated because of the higher permeability of the green body. As an example, multilayer ceramic capacitors (MLCs) processed by a sequential supercritical and then thermal processing route exhibited no change in electrical properties as compared to MLCs processed solely by a thermal binder removal process [8].

Part of the attractiveness of supercritical extraction stems from the recognition that it may be used to avoid two problems associated with thermal debinding, namely, that thermal cycles may be long and that defects may occur in the green body due to pressure buildup as binder is decomposed. These advantages arise because of the differences in the mechanisms associated with the two processes. In thermal debinding, the kinetic decomposition of the solid binder causes a phase change of the organic species

to gas- or liquid-phase molecules, and such molecules then either diffuse through binder-filled, closed pore space or are driven by forced convection through open porosity as the pressure builds within the green body. The occurrence of pressure gradients may then lead to stress and ultimately to failure of the green body [14-17]. The difficulty in thermal debinding thus becomes in developing a heating schedule that finds a balance between the timely removal of binder without the introduction of defects into the green body.

In contrast to thermal debinding, the mechanism of binder removal during supercritical extraction is one of solvation of the binder molecules by the supercritical fluid followed by constant pressure diffusion either through the binder-filled pore space or through open pores. The process of supercritical extraction may be conducted in one of two modes, which have ramification on the success of the process. In the first, a continuous mode of operation is employed whereby fresh fluid is continuously fed to the vessel as binder-laden supercritical fluid is withdrawn—such a process is thus isobaric, and pressure gradients, and hence defects, do not arise during the extraction segment of the cycle. Alternatively, a quasi-batch (or semi-continuous) process may be used whereby the vessel is first pressurized, followed by a constant pressure extraction segment, and then a depressurization step is used [8,9,13]; these three steps are then repeated. This latter approach may help to facilitate the removal of binder by having the binder-laden supercritical fluid be convected from the green body during depressurization, as compared to a pure Fickian diffusion process at constant pressure.

Regardless of the mode of extraction employed, the final depressurization of the vessel to ambient conditions always leads to pressure gradients within the sample, which may ultimately lead to stress and defects in the samples [13]. When depressurization is

very rapid and heat transfer is low, the venting of the supercritical fluid from the vessel corresponds to a Joule-Thompson expansion with a concomitant decrease in temperature, which if too extreme can lead to the formation of dry ice, both within the vessel and within the sample. The subsequent sublimation of this dry ice then leads to internal pressure within the green body, which leads to defects such as cracking and delamination. A second mechanism for defect formation is that during depressurization of the vessel—even when conducted relatively slowly and/or with sufficient heat transfer so as to avoid a large temperature decrease—the finite permeability of the green body leads to pressure gradients within the sample, the occurrence of which leads to stress and may ultimately lead to failure.

In this work, we focus on the latter type of failure mechanism, *i.e.*, pressure gradients that arise during isothermal depressurization, and we present the conditions under which such defects occur. We then develop a 1-D model for flow in porous media to describe the temporal and spatial evolution of pressure during the isothermal depressurization step. The resulting unsteady-state, non-linear differential equation is next solved numerically, and we also account for additional complications that arise from operating at supercritical conditions, namely, that the fluid is non-ideal and must be described a cubic equation of state and that the viscosity of supercritical carbon dioxide is a moderately strong function of pressure. The model is then used to help explain the origin of the failure behavior. We also compare the pressure gradients that arise in green bodies during depressurization from supercritical conditions to those that arise during thermal debinding.

3.2 EXPERIMENTAL

Two types of multilayer components were evaluated in this work. For the first, designated as Sample A, tapes nominally consisted of 89.1 weight% of a BaTiO₃-based N2200 dielectric, 9.9 weight% acrylic-based resin (B72, Rohm & Haas, Ontario, Canada), and 2 weight% polyester adipate plasticizer (G50, C. P. Hall, Bedford Park, IL). The individual green tapes were laminated into multilayer ceramic capacitors (MLCs) that had 41 active layers and Pt/Pd/Au electrodes. The dimensions of the MLC after lamination were 2.2×2.0×1.0 cm. The porosity of the MLCs was 0.10, as determined by Archimedes' method, and the permeability of five green tapes (laminated at 29 MPa at 85°C for 10 min) was determined from flux measurements as $\sim 8 \times 10^{-19} \text{ m}^2$, using a procedure described in more detail elsewhere [18,19].

For the second type of sample (Sample B), the tapes nominally consisted of 87.2 weight% BaTiO₃ (X7R422H, Ferro, Niagara Falls, NY), 6.55 weight% poly (vinyl butyral) resin, (PVB BL-1, Sekisui, Troy, MI) and 5.3 weight% dioctyl phthalate (DOP). The individual green tapes were laminated at 7 MPa at 85°C for 10 min into multilayer bodies that had 45 layers; the dimensions after lamination were 2.1×1.5×0.17 cm. The porosity of the MLCs before extraction was 0.07 (0.18 after extraction) as determined by Archimedes' method. The permeability of 1 unlaminated green tape was determined from flux measurements as $\sim 2 \times 10^{-18} \text{ m}^2$ before extraction, and is estimated to be a factor of 5 larger due to the combined effects of lamination and extraction.

For the extraction experiments, a 316 stainless steel, 500 ml Parr vessel was used which was equipped with a thermocouple located in a well in the vessel cover. The vessel was placed in a constant-temperature bath and was maintained within $\pm 1^\circ\text{C}$ and

± 0.5 MPa. Carbon dioxide was used as the supercritical fluid at temperatures of 50-90°C and pressures of 10-40 MPa. The extraction experiments were performed in a semi-continuous mode with the green samples exposed to charges of supercritical fluid each lasting 1 hour. To control the rate of depressurization from conditions of supercritical extraction, a vent valve was adjusted to achieve depressurization over times of 0.5-24 h and for these values, the temperature varied by most 1-2 degrees Celsius. After the extraction process, the amount of organic fraction removed was determined from the weight loss of the samples, normalized by the total amount of organic phase initially present.

3.3 MODEL

To develop a 1-D model for describing the pressure distribution in the green body of overall length, L , we make the following assumptions. 1) The green body is a porous continuum consisting of volume fractions of solid, ε_s , binder, ε_b , and void, ε_v , which are related by $\varepsilon_s + \varepsilon_b + \varepsilon_v = 1$. 2) During depressurization, both, the dimensions of the green body and the volume fractions remain unchanged. This latter statement does not preclude that ε_b may change as a consequence of extraction, but only that substantial further extraction does not occur as gas is exiting the vessel. 3) The properties of the supercritical fluid can be modeled as that of pure carbon dioxide, which is justified in light of the low binder concentrations of approximately < 0.01 weight% present in the supercritical phase. 4) For flow in porous media from the conditions of supercritical extraction, the velocity of a compressible fluid is given by Darcy's Law. 5) The process proceeds isothermally.

From Darcy's Law, the flow of carbon dioxide in the porous green body can be written in terms of the superficial fluid velocity, v , in the x direction as [20]

$$v = -\frac{\kappa}{\mu} \frac{\partial P}{\partial x} \quad (3.1)$$

where κ is the permeability of the sample, μ is the viscosity of the fluid, and P is the pressure, which can ultimately be related to the gas molar density, ρ , of a compressible fluid. The continuity equation for the fluid in the green body is given by

$$\frac{\partial(\rho \varepsilon_v)}{\partial t} = -\frac{\partial}{\partial x}(\rho v) \quad (3.2)$$

where t is the time. Substitution of Eq. 3.1 into Eq. 3.2 then leads to

$$\frac{\partial(\rho \varepsilon_v)}{\partial t} = \frac{\partial}{\partial x} \left(\rho \frac{\kappa}{\mu} \frac{\partial P}{\partial x} \right) \quad (3.3)$$

To proceed further, we use a relationship between the molar density and the pressure, which can be obtained from a generic cubic equation of state as [21]

$$P = \frac{RT}{V - b} - \frac{a}{(V + \sigma b)(V + \epsilon b)} \quad (3.4)$$

where $V=1/\rho$ is the molar volume, and a , b , ϵ , and σ are the constants specific to the cubic equation of state. In this work, we use the Peng-Robinson equation of state [21,22], and although the model results are obtained in terms of the molar density, for convenience the results are converted to pressure via Eq. 3.4.

Because of the large range of pressures traversed during depressurization, the viscosity of carbon dioxide cannot be taken as a constant [23], and thus we express the viscosity as a quadratic equation in the molar density

$$\mu(\rho) = a^* \rho^2 + b^* \rho + c^* \quad (3.5)$$

where $a^* = 1.7 \times 10^{-13}$ Pa s m⁶/mol², $b^* = 8.2 \times 10^{-11}$ Pa s m³/mol, and $c^* = 1.8 \times 10^{-5}$ Pa s are constants. Figure 3.1 shows that this parameterization adequately describes the viscosity over a range of molar density, and hence pressures of 0.1-40 MPa, at 90°C.

Equations 3.3 – 3.5 were solved by a Forward Time Centered Space Technique as an explicit method [24], subject to the initial condition that $\rho = \rho^o$ at $t=0$. At the edges of the 1-D body of overall length, L , the boundary condition was of a linear decrease in the boundary density with time given by $\rho(\pm L/2, t) = \rho^o - \alpha \times t$, where α is a constant.

To explore some general behavior of the governing differential equation, Eq. 3.3 can be rewritten for the case of a constant viscosity and of an ideal gas where $\rho = P/RT$, and then made dimensionless with the substitutions $\bar{x} = \frac{2x}{L}$, $\bar{\rho} = \frac{\rho}{\rho^o}$, and $\bar{t} = \frac{t}{\gamma}$, where

$$\gamma = \frac{\mu \varepsilon_v L^2}{4\kappa RT \rho^o} \quad (3.6)$$

is the time constant for the depressurization process. The form of the time constant indicates that large body size or small permeability or a combination of both will lead to long depressurization cycles to avoid the buildup of pressure. With these substitutions, the governing differential equation becomes

$$\frac{\partial \bar{\rho}}{\partial \bar{t}} = \frac{\partial \left(\bar{\rho} \frac{\partial \bar{\rho}}{\partial \bar{x}} \right)}{\partial \bar{x}} \quad (3.7)$$

with the initial condition that at $\bar{t} = 0$, $\bar{\rho} = 1$ and that the boundary condition for linear depressurization is that at $\bar{x} = \pm 1$, $\bar{\rho}(1, \bar{t}) = 1 - \alpha \gamma \bar{t} / \rho^o$.

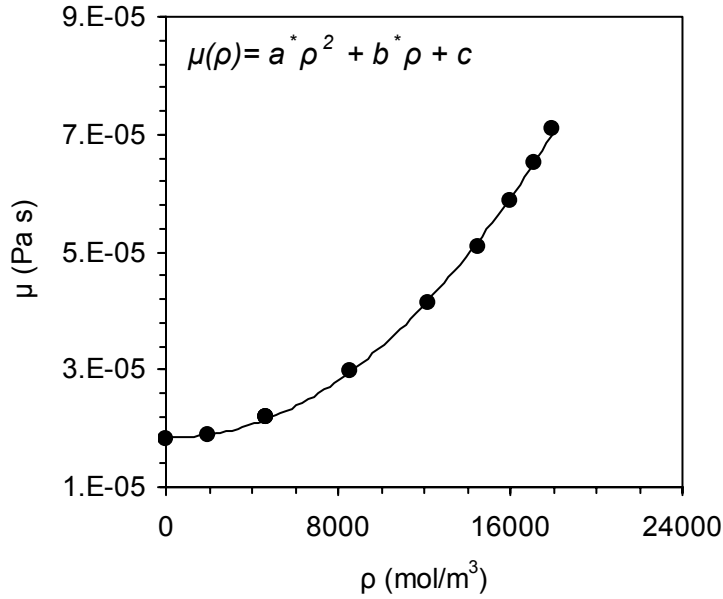


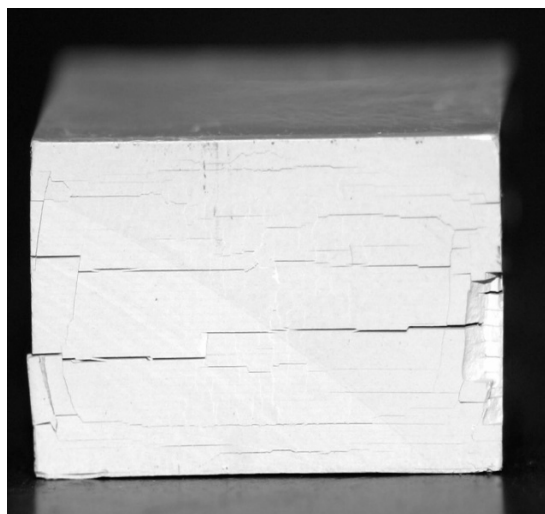
Figure 3.1: Viscosity of carbon dioxide versus molar density at 90°C. Data are adopted from Ref. [23] and the regression curve is indicated by the solid line.

3.4 RESULTS AND DISCUSSION

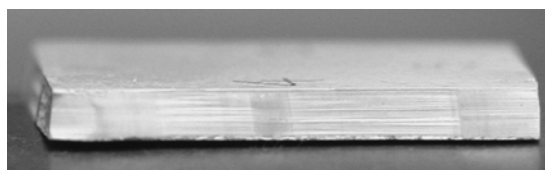
The two types of samples evaluated were subjected to extraction conditions in supercritical carbon dioxide of 40 MPa at 90°C for 1 h. Composition A of the acrylic-based binder experienced ~10% weight loss based on the total binder content. Figure 3.2a is an image of a sample after depressurization over 24 h. Severe horizontal and vertical cracks are evident, with many of the horizontal defects arising as delamination at the electrode layers. Both the number and width of the cracks are largest along the mid-plane of the MLC, and this central location of defects was also evident in samples that experienced cracking from other conditions of depressurization over the range of conditions from 10-40 MPa and 55-90°C. For PVB/DOP Composition B, the multilayer sample experienced approximately ~27% weight loss of the total binder content after exposure to supercritical carbon dioxide at 40 MPa at 90°C for 1 h. Figure 3.2b shows that no cracking of the sample is evident after depressurization over 6 h.

The model is next used to examine how the pressure varies temporally and spatially in the green body during depressurization from a body of 2 cm in length with a low permeability of 10^{-18} m^2 (see Table 3.1 for other model parameters). Figure 3.3 shows the time evolution of the pressure of CO₂ versus position in the sample for a depressurization time of $t^{DP}=0.2 \text{ h}$ (left-hand side of Figure 3.3) versus $t^{DP}=6 \text{ h}$ (right-hand side of Figure 3.3). For the more rapid rate of depressurization, variations in pressure exist within the sample, with the pressure being largest at the center of the sample and lowest at the body edges. The pressure gradients within the sample, however, are largest near the body edges, and these become more pronounced as depressurization proceeds. The behavior in pressure indicates that for a faster rate of depressurization, the

rate of convection arising from the pressure gradients is too slow as compared to the rate of depressurization of the vessel. For the slower rate of depressurization, the pressure distribution within the sample are more uniform for all times, which indicates that rate of forced convection is sufficient maintain more uniform pressure within the green body.



a



b

Figure 3.2: Images of Sample A (above) after depressurization over 24 h and Sample B (below) after depressurization over 6 h from conditions of supercritical extraction in carbon dioxide at 90°C and 40 MPa for 1 h.

Table 3.1: Summary of parameter values used for Figs. 3.3 – 3.8.

Parameters (Units)	Values			
	Figs. 3.3, 3.4	Figs. 3.5, 3.6	Fig. 3.7	Fig. 3.8
κ (m ²)	1×10^{-18}	1×10^{-16}	varies	1×10^{-17}
ε (-)	0.1	0.15	0.15	0.15
L (m)	0.02	0.02	0.02	varies
t^{DP} (h)	0.2, 6	0.2, 6	0.2	0.2
t (h)	varies	varies	0.1, 0.2	0.1, 0.2

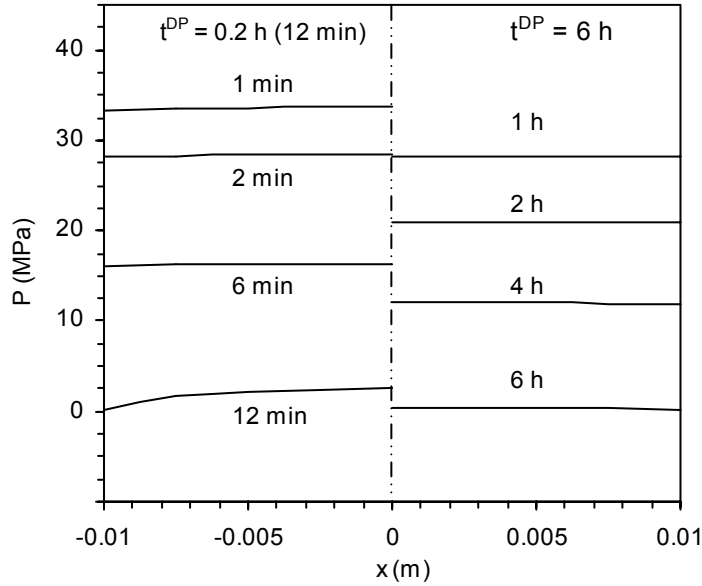


Figure 3.3: Pressure of CO₂ at 90°C versus position in the green body as a function of time for $\kappa=10^{-18}$ m² and $\varepsilon_v=0.10$. The left-hand side corresponds to a depressurization time of $t^{DP}=0.2$ h, and the right-hand side corresponds to a depressurization time of $t^{DP}=6$ h.

In earlier work in the modeling of thermal debinding [16,17], we have shown that the pressure in the center of the body is largest and that the pressure gradients are largest at the edges of the body, which is qualitatively similar to what is seen in Figure 3.3 during depressurization from conditions of supercritical extraction. We have also shown that the stress within the sample is proportional to the gradient in pressure within the sample [17], and that the maximum in the stress coincides with occurrence of the maximum relative pressure in the center of the green body. To develop a measure that reflects in part these two observations, we define a normalized pressure ratio, $P_{n,x}$, as the ratio of the pressure at any position in the body, P_x , to the pressure at the body edge, $P_{x=\pm L/2}$, as

$$P_{n,x} = \frac{P_x}{P_{x=\pm L/2}} \quad (3.8)$$

Thus, large values of $P_{n,x}$ indicate a large relative pressure and also large pressure gradients in the green body. For thermal debinding, even small values of $P_{n,x}$ of >1.01 were calculated at failure [25], but the absolute magnitude of such values are uncertain in light of uncertainty in model parameters and because of the tight coupling between many different model parameters, as described in more detail elsewhere [25-27]. Nevertheless, it is possible that even modest values of $P_{n,x}$ may increase the likelihood of failure of the green body, as the strength of green bodies is low, especially as binder is removed.

Figure 3.4 shows how $P_{n,x}$ varies spatially and temporally for the rapid and slow linear rates of depressurization shown in Figure 3.3. For rapid depressurization times up to 6 min, $P_{n,x}$ is initially slightly higher in the center of the body and decreases across the body thickness. With increasing time, $P_{n,x}$ versus position in the body becomes larger and approaches a value of 24 as the depressurization segment ends, which may suggest

that failure may occur late in the depressurization segment. For a slower rate of depressurization, the temporal behavior of $P_{n,x}$ is qualitatively similar, but now, however, $P_{n,x}$ is much smaller in magnitude as compared to more rapid depressurization.

The results of a similar set of simulations are shown in Figure 3.5 but now for a body of higher permeability of 10^{-16} m^2 . Once again, qualitatively similar behavior in the pressure profiles is observed in Figure 3.5 as compared to Figure 3.3. The main difference, however, is that gradients across the green body are much smaller, and this is reflected in the smaller values of $P_{n,x}$ in Figure 3.6.

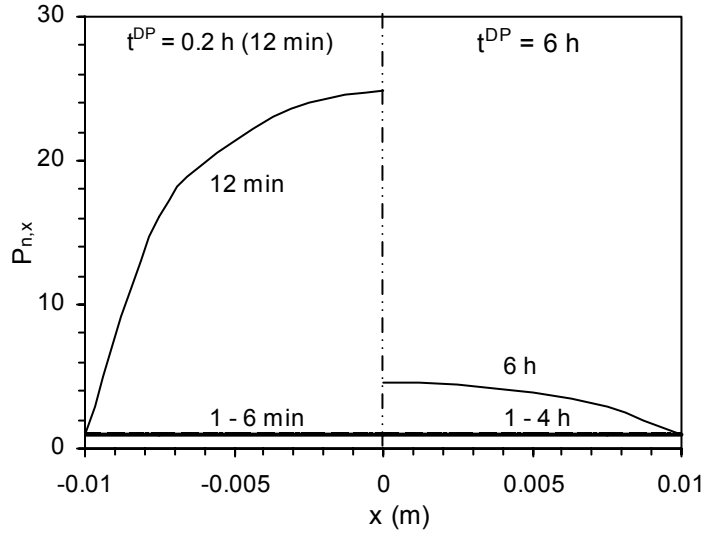


Figure 3.4: Behavior of $P_{n,x}$ of CO_2 at 90°C versus position in the green body as a function of time for $\kappa=10^{-18} \text{ m}^2$ and $\varepsilon_v=0.10$. The left-hand side corresponds to a depressurization time of $t^{DP}=0.2 \text{ h}$, and the right-hand side corresponds to a depressurization time of $t^{DP}=6 \text{ h}$.

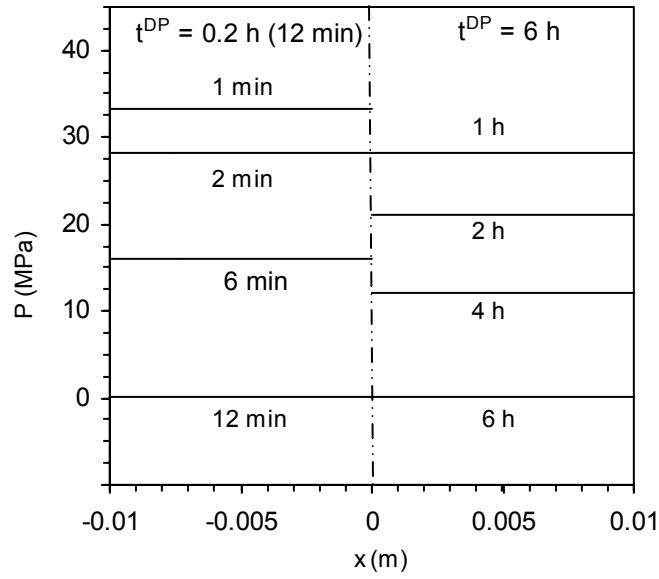


Figure 3.5: Pressure of CO₂ at 90°C versus position in the green body as a function of time for $\kappa=10^{-16}$ m² and $\varepsilon_v=0.15$. The left-hand side corresponds to a depressurization time of $t^{DP}=0.2$ h, and the right-hand side corresponds to a depressurization time of $t^{DP}=6$ h.

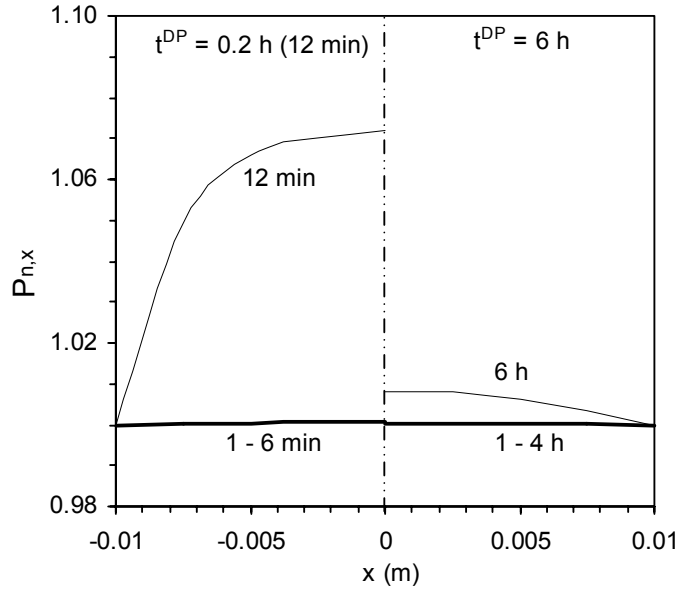


Figure 3.6: Behavior of $P_{n,x}$ of CO_2 at 90°C versus position in the green body as a function of time for $\kappa=10^{-16} \text{ m}^2$ and $\varepsilon_v=0.15$. The left-hand side corresponds to a depressurization time of $t^{DP}=0.2 \text{ h}$ and the right-hand side corresponds to a depressurization time of $t^{DP}=6 \text{ h}$.

To explore a wider range of parameters, the effects of the permeability of a body of constant length of 2 cm on the pressure within the green body was examined. Figure 3.7 thus shows the effect of the permeability on the pressure distribution for depressurization times lasting $t^{DP}=0.2 \text{ h}$ and for times corresponding to the midpoint ($t=0.1 \text{ h}$, left-hand side) and endpoint ($t=0.2 \text{ h}$, right-hand side) of the depressurization ramp. For both times, larger pressures and pressure gradients arise when the permeability is low. Once again, we also see that the pressure gradient becomes more severe with longer time. These model results are thus qualitatively consistent with the occurrence of defects in Sample A, which undergoes little extraction and has low permeability, as compared to Sample B, which undergoes significant extraction and has higher permeability.

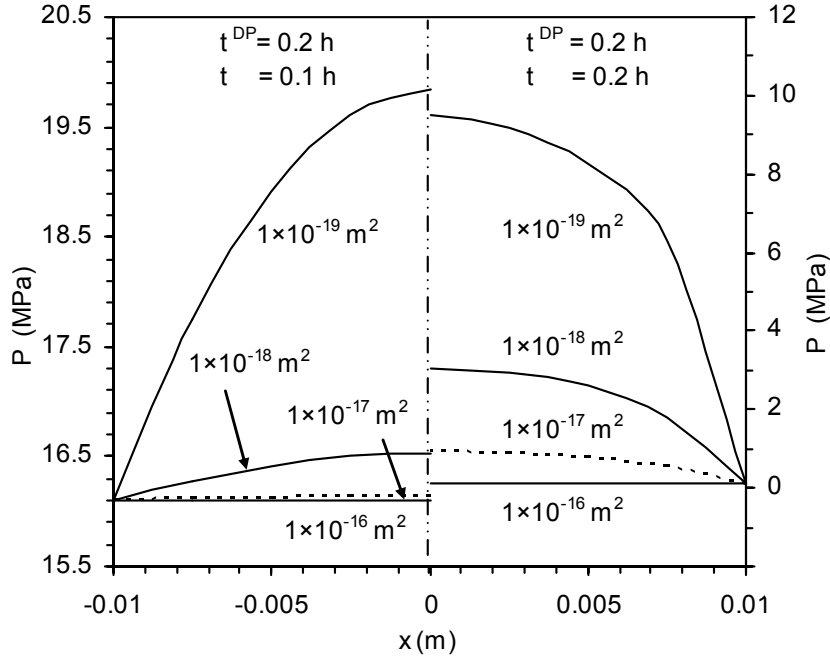


Figure 3.7: Effect of permeability on the pressure of CO₂ at 90°C versus position in the green body for linear depressurization of $t^{DP}=0.2$ h at $t=0.1$ h (left-hand side) and for $t=0.2$ h (right-hand side).

The effect of sample length on the depressurization behavior is explored in Figure 3.8, which shows that for a fixed permeability and linear depressurization, the pressures and pressure gradients in the green body are substantially larger for larger sized components, with increasing time, the pressure gradients within the green body become more pronounced. A similar effect of sample size on the pressure and pressure gradients was observed when modeling the pressure in green bodies during thermal binder removal [16].

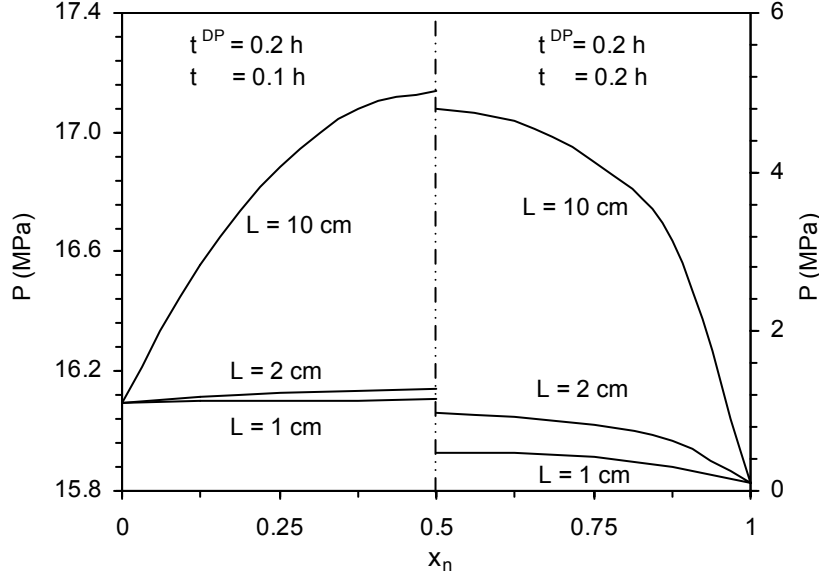


Figure 3.8: Effect of sample length scale on the pressure of CO₂ at 90°C versus dimensionless position in the green body for linear depressurization of $t^{DP}=0.2$ h at $t=0.1$ h (left-hand side) and for $t=0.2$ h (right-hand side).

To summarize a broad range of depressurization behavior, the non-dimensional differential equation (Eq. 3.7) was solved for a linear depressurization over 0.2 h for a range of values of the time constant for depressurization, γ . For typical ceramic body dimensions of 0.1-0.001 m and for permeabilities of $10^{-16} - 10^{-19}$ m², γ ranges from 0.001-1000 s. Figure 3.9 shows that large values of γ —which imply either a large body or small permeability or both—lead to small changes in pressure at the center, and thus throughout, the green body with time; the corresponding values of relative pressure and pressure gradients will be large with concomitant higher stress and higher probability of failure. Figure 3.10 shows explicitly how the quantity $P_{n,x=0}$ varies with time. For larger values of the time constant, $P_{n,x=0}$ is larger for all times and becomes largest at the end of the depressurization ramp. For Sample A and Sample B examined here, γ is of order ~ 8 s and ~ 0.2 s, respectively, which is a ratio of ~ 40 in the time constant. This ratio is

consistent with slower depressurization behavior and hence larger relative pressure and larger pressure gradients within Sample A, and thus with an enhanced propensity for failure.

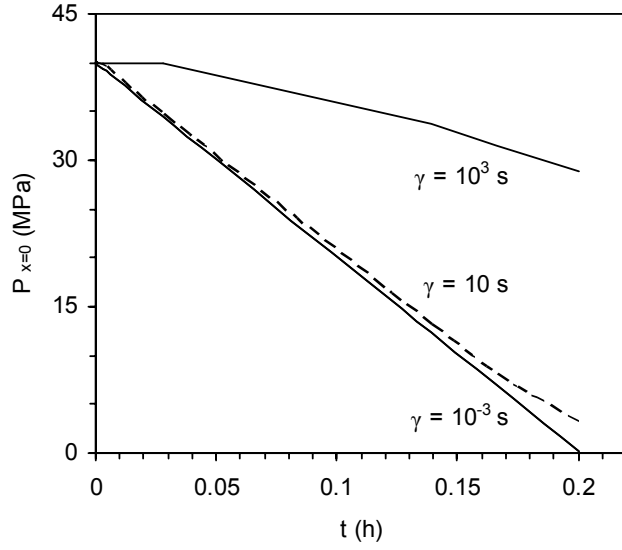


Figure 3.9: Behavior of $P_{x=0}$ of CO_2 at 90°C versus time for linear depressurization of $t^{DP}=0.2$ h for different values of γ .

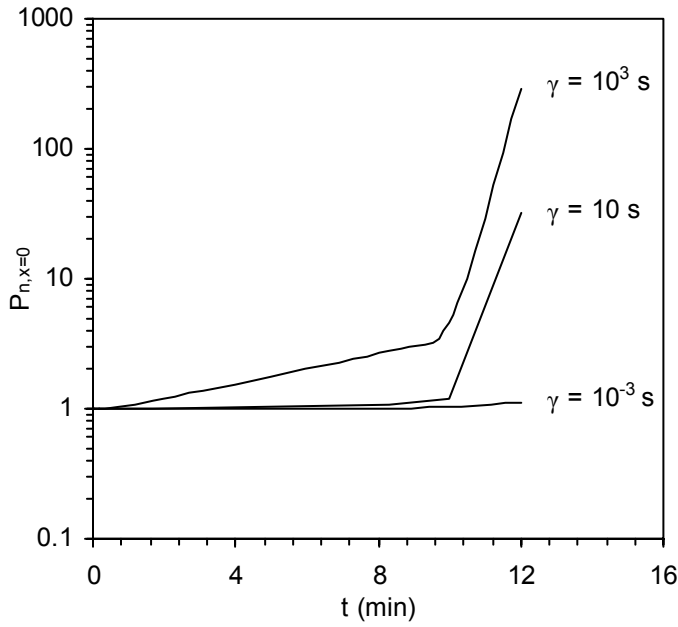


Figure 3.10: Behavior of $P_{n,x=0}$ of CO_2 at 90°C versus time for linear depressurization of $t^{DP}=0.2$ h for different values of γ .

In summary, although supercritical extraction is an alternative means to rapidly remove binder from green ceramic components, the occurrence of defects such as cracking and delamination is also possible. In this work, we attribute the origin of such defects to enhanced pressure within the sample relative to the pressure in the vessel, and to associated pressure gradients within the green body which arise during depressurization from the conditions of supercritical extraction.

Although the model presented to quantify the pressure within green bodies during depressurization is highly simplified, it does allow for both a quantitative and qualitative assessment of the pressure profiles within the green body as a function of depressurization time. In light of the results presented here, several of the assumptions inherent in the model can be examined. Most importantly, the use of Darcy's Law implies laminar flow, and this assumption can be examined by examination of the Reynolds number, $N_{Re} = \rho v D / \mu$ where v can be determined from Eq. 3.1 once the gradient in pressure is known. For the range of parameters examined here, $N_{Re} < 1$, and thus laminar flow prevails. For situations in which the Reynolds number were high, turbulent flow could be included in the model, but this would only serve to enhance flow and decrease the pressure and pressure gradients within the green body.

A further refinement to the model would be to explicitly account for the occurrence of slip flow in pores of small size, although this mechanism would not be operative at high pressure where the mean free path in the supercritical phase is low because the supercritical fluid density is comparable to that of liquids. Thus, slip flow would only become relevant late in the depressurization cycle as the pressure becomes low and the mean free path large, relative to the pore size. Non-isothermal flow could

also be considered for very fast depressurization times, but this would introduce additional complexity to the model. Finally, although more complicated models exist for describing flow in porous media [20,28,29], these often require values of parameters that are not easily obtained.

Thus, in spite of the simplifications invoked here, the model likely captures the two most important quantities in the depressurization process, namely, the length scale of the body and the permeability, and the combined effect of these two quantities is reflected in the time constant for flow. The inclusion of more complicated flow behavior will likely not qualitatively change the main results presented here, and thus the model developed and presented here is a useful tool to assess under what circumstances the depressurization process is likely to be a concern.

3.5 CONCLUSIONS

Defects in ceramic green bodies containing binder have been shown to occur during the process of supercritical extraction of binder. A model based on flow in porous media has been developed to describe the spatial and temporal distribution of pressure within green bodies during the depressurization process. The model thus contains two important parameters, namely, the length scale of the body and the permeability, and thus describes their effect on the spatial and temporal development of pressure and pressure gradients within green bodies. The results from the model are qualitatively consistent with the observance of defects in green bodies that contain binders that exhibit low solubility in supercritical carbon dioxide and also have low permeability.

3.6 REFERENCES

1. S. Nakajima, S. Yasuhara, and M. Ishihara, "Method of Removing Binder Material from a Shaped Ceramic Preform by Extracting with Supercritical Fluid," US Patent No. 4,731,208, March 15, 1988.
2. T. Miyashita, Y. Ueno, H. Nishio, and S. Kubodera, "Method for Removing the Dispersion Medium from a Molded Pulverulent Material," US Patent No. 4,737,332, April 12, 1988.
3. D. W. Matson and R. D. Smith, "Supercritical Fluid Technologies for Ceramic-Processing Applications," *J. Am. Ceram. Soc.*, **72** [6] 871-881 (1989).
4. E. Nishikawa, N. Wakao and N. Nakashima, "Binder Removal from Ceramic Green Body in the Environment of Supercritical Carbon Dioxide with and without Entrainers," *J. Supercrit. Fluids*, **4** 265-269 (1991).
5. T. Chartier, M. Ferrato and J. F. Baumard, "Supercritical Debinding of Injection Molded Ceramics," *J. Am. Ceram. Soc.*, **78** [7] 1787-92 (1995).
6. T. Chartier, E. Delhomme and J. Baumard, "Mechanisms of Binder Removal Involved of Injection Molded Ceramics," *J. De Physique III*, **7** [2], 291-02 (1997).
7. T. Chartier, E. Delhomme, J. F. Baumard, P. Marteau, P. Subra and R. Tufeu, "Solubility in Supercritical Carbon Dioxide, of Paraffin Waxes Used as Binders for Low-Pressure Injection Molding," *Ind. Eng. Chem. Res.*, **38** [5] 1904-10 (1999).
8. R. V. Shende, D. S. Krueger and S. J. Lombardo, "Supercritical Extraction of Binder Containing Poly(vinyl butyral) and Dioctyl Phthalate from Barium

- Titanate-Platinum Multilayer Ceramic Capacitors,” *J. Mater. Sci.: Mater. Electron.*, **12** 637-643 (2001).
9. R. V. Shende and S. J. Lombardo, “Supercritical Extraction with Carbon Dioxide and Ethylene of Poly(vinyl butyral) and Dioctyl Phthalate from Multilayer Ceramic Capacitors,” *J. Supercrit. Fluids*, **23** 153-162 (2002).
 10. F. Bordet, T. Chartier, J. F. Baumard, “The Use of Co-Solvents in Supercritical Debinding of Ceramics,” *J. European Ceram. Soc.*, **22** 1067-1072 (2002).
 11. T. Chartier, F. Border, E. Delhomme, J. F. Baumard, “Extraction of Binders from Green Ceramic Bodies by Supercritical Fluid: Influence of the Porosity” *J. European Ceram. Soc.*, **22** 1403-1409 (2002).
 12. R. V. Shende, M. Kline and S. J. Lombardo, “Effects of supercritical extraction on the plasticization of poly(vinyl butyral) and dioctyl phthalate films,” *J. Supercrit. Fluids*, **28** 113-120 (2004).
 13. R. V. Shende, T. R. Redfern and S. J. Lombardo, “Defect Formation during Supercritical Extraction of Binder from Green Ceramic Components,” *J. Am. Ceram. Soc.*, **87** [7] 1254-1258 (2004).
 14. G. Y. Stangle, and I. A. Aksay, “Simultaneous Momentum, Heat and Mass Transfer With Chemical Reaction in a Disordered Porous Medium: Application to Binder Removal from a Ceramic Green Body,” *Chem. Eng. Sci.*, **45** 1719-1731 (1990).
 15. D-S. Tsai, “Pressure Buildup and Internal Stresses During Binder Burnout: Numerical Analysis,” *AIChE J.*, **37** [4] 547-554 (1991).

16. S. J. Lombardo and Z. C. Feng, "Pressure Distribution during Binder Burnout in Three-Dimensional Porous Ceramic Bodies with Anisotropic Permeability," *J. Mat. Res.*, **17** 1434-1440 (2002).
17. Z. C. Feng, B. He, and S. J. Lombardo, "Stress Distribution in Porous Ceramic Bodies During Binder Burnout," *J. of Appl. Mech.*, **69** 497-501 (2002).
18. J. W. Yun and S. J. Lombardo, "Permeability of Green Ceramic Tapes as a Function of Binder Loading," *J. Am. Ceram. Soc.*, **90** [2] 456-461 (2007).
19. J. W. Yun and S. J. Lombardo, "Permeability of Laminated Green Ceramic Tapes as a Function of Binder Loading," *J. Am. Ceram. Soc.*, **91** [5] 1553-1558 (2008).
20. R. B. Bird, W. E. Stewart, and E. N. Lightfoot, *Transport Phenomena*, 1st Ed., John Wiley & Sons, New York, 1960.
21. J. M. Smith, H. C. Van Ness and M. M. Abbott, *Introduction to Chemical Engineering Thermodynamics*, 6th Ed., McGraw Hill, New York, 2001.
22. D.-Y. Peng and D. B. Robinson, "A New Two-Constant Equation of State" *Ind. Eng. Chem. Fundam.*, **15** [1] 59-64 (1976).
23. A. Fenghour, W.A. Wakeham and V. Vesovic, "The Viscosity of Carbon Dioxide," *J. Phys. Chem. Ref. Data*, **27** [1] 31-44 (1998).
24. A. L. Garcia, *Numerical Methods for Physics*, 2nd Ed, Prentice Hall, New Jersey, 2000.
25. J. W. Yun and S. J. Lombardo "Methods for Introducing Safety Factors into Minimum Time Heating Cycles for Binder Removal from Green Ceramic Bodies," *J. Ceram. Proc. Res.*, **8** 402-410 (2007).

26. J. W. Yun, D. S. Krueger, P. Scheuer, and S. J. Lombardo “Effect of Decomposition Kinetics and Failure Criteria on Binder Removal Cycles From Three-Dimensional Porous Green Bodies,” *J. Am. Ceram. Soc.*, **89** [1] 176-183 (2006).
27. J. W. Yun and S. J. Lombardo “Determination of Rapid Heating Cycles for Binder Removal from Open-Pore Green Ceramic Components,” accepted to *Advances in Applied Ceramics* (2008).
28. F. Thuavin and K. K. Mohanty, “Network Modeling of Non-Darcy Flow Through Porous Media,” *Transport Porous Media*, **31** 19-37 (1998).
29. K. Kannan and K. R. Rajagopal, “Flow through Porous Media due to High Pressure Gradients,” *App. Math. Comput.*, **199** 748-759 (2008).

CHAPTER 4

CONCLUSIONS AND FUTURE WORK

4.1 CONCLUSIONS

Supercritical extraction was performed using carbon dioxide as the supercritical fluid on acrylic-based multilayer ceramic systems and the results were compared with a poly (vinyl butyral)-based multilayer ceramic system. The solubility of the corresponding resins and the plasticizers of both binder systems were of the same order of magnitude, although the solubility of the plasticizers was much higher than that of the resins. Extraction experiments on individual binder components of the acrylic-based system showed the presence of interactions between the components when present in the same extraction vessel. The contribution to overall weight loss of binder for this system was therefore from the plasticizer as well as the resin.

For enhancing supercritical extraction, co-solvents were evaluated and optimization of the co-solvent loading in the supercritical fluid was performed. Diffusivity calculations of the extractable binder component for both binder systems was found to be of the same order of magnitude, but numerically the value of diffusivity for the acrylic-based binder system was thrice as high. This may have been due to the presence of defects in the samples after supercritical extraction. Therefore a visual analysis of the samples with defects followed, and a mechanism for defect formation was suggested.

To quantify the defect formation in green ceramic bodies containing binder, a model based on flow in porous media was developed. This model contains two important parameters, namely the length scale and the gas-phase permeability. The effects of permeability and length scale were investigated on the spatial and temporal development

of pressure during depressurization, the results of which were qualitatively consistent with experimental observations.

4.2 FUTURE WORK

Supercritical extraction on acrylic-based multilayer ceramic capacitors always resulted in defect formation. The occurrence of defects was due to the lack of sample permeability, which increased the equilibration lag-time between the sample and its surrounding supercritical phase during depressurization. Since depressurization can not be avoided altogether, the most effective way to avoid defects would be to increase the sample permeability before the first depressurization. After the first 1-h cycle of supercritical extraction at 90°C and 40 MPa, ~3.5% binder was extracted, which resulted in a very modest increase in sample permeability. To increase sample permeability, the strategy would be to extract additional binder that is not extractable at 90°C and 40 MPa.

The technique to extract additional binder can therefore be, to utilize the effect of increasing temperature in a high pressure environment to increase the binder weight loss, as has been mentioned in Refs. [1-4], up to an upper temperature limit, above which, thermal degradation of binder occurs. If operating at 40 MPa, switching to a higher temperature without depressurizing the vessel would result in expansion of the supercritical fluid in the vessel beyond the vessel's capabilities, which is always undesirable. This issue can be circumvented by (i) either performing the first step of supercritical extraction at pressures less than 40 MPa and then rising in temperature or by (ii) simultaneously heating and depressurizing the vessel such that, in spite of the increasing vessel temperature, the pressure in the vessel remains constant at 40 MPa.

Solubility values for the acrylic-based binder system have not been reported at high temperatures because it is not known at what temperatures they start to degrade in a high pressure environment. An important area of investigation would therefore be to

determine the upper limit of the operating temperature for supercritical extraction such that weight loss of binder is still extraction controlled. With this information at hand, supercritical extraction experiments can be performed at higher temperatures to extract additional binder in comparison to the binder extracted at 90°C and 40 MPa, to aim at generating more open pore space within the green ceramic.

When operating in a semi-continuous mode, the supercritical fluid eventually gets saturated with binder, which inhibits further extraction. Thus depressurization has to be performed to remove the binder-laden supercritical fluid and charge in more fresh solvent. Chapter 2 has already shown that due to lack of available sample permeability, the sample undergoes defects during depressurization. To delay depressurization, a continuous mode of extraction will have to be used. When operating in a continuous mode, depressurization does not need to be conducted until extraction of binder from the sample has ceased, at which point the permeability will be higher. Combination of higher temperature supercritical extraction along with operating the vessel in a continuous mode would render more binder being extracted from the sample and would avoid saturation of the supercritical phase.

4.3 REFERENCES

1. R. V. Shende, D. S. Krueger and S. J. Lombardo, "Supercritical Extraction of Binder Containing Poly (vinyl butyral) and Dioctyl Phthalate from Barium Titanate-Platinum Multilayer Ceramic Capacitors," *J. Mater. Sci.: Mater. Electron.*, **12** 637-643 (2001).
2. R. V. Shende and S. J. Lombardo, "Supercritical Extraction with Carbon Dioxide and Ethylene of Poly(vinyl butyral) and Dioctyl Phthalate from Multilayer Ceramic Capacitors," *J. Supercrit. Fluids*, **23** 153-162 (2002).
3. R. V. Shende, M. Kline and S. J. Lombardo, "Effects of supercritical extraction on the plasticization of poly (vinyl butyral) and dioctyl phthalate films," *J. Supercrit. Fluids*, **28** 113-120 (2004).
4. R. V. Shende, T. R. Redfern and S. J. Lombardo, "Defect Formation during Supercritical Extraction of Binder from Green Ceramic Components," *J. Am. Ceram. Soc.*, **87** [7] 1254-1258 (2004).

APPENDIX

**NUMERICAL TECHNIQUE USED FOR CALCULATING SPATIAL
AND TEMPORAL DISTRIBUTION OF PRESSURE IN GREEN
CERAMIC BODIES DURING DEPRESSURIZATION**

A.1 INTRODUCTION

Chapter 3 dealt with the development of a mathematical model that describes the spatial and temporal distribution of pressure within the body due to equilibration lag time between the supercritical fluid in the sample and its surrounding, during depressurization from conditions of supercritical extraction. This model was based on flow in porous media that accounted for the characteristics of the ceramic sample, operating conditions of supercritical extraction at the initiation of depressurization as well as the rate of depressurization to estimate the relative pressure and the associated pressure gradients within the green body. The resulting governing equation of the model was a partial differential equation in position, x , and time, t , with density, ρ , of CO₂ as the dependent variable. Since depressurization was a time-dependent process, the pressure of CO₂ at the edge of the sample was also time-dependent. The boundary conditions for the governing equation were therefore non-homogeneous in nature.

On accounting for the change in viscosity of CO₂ in the vessel with pressure [1] during depressurization and taking into consideration the non-ideal behavior of CO₂ at high pressures [2,3], the governing equation was a non-linear partial differential equation which had to be solved with the non-homogeneous boundary conditions. Analytical solutions for such equations are not easily obtainable. Thus, the numerical technique of Forward Time Centered Space (FTCS) [4] was used. This technique used a forward derivative in time and central derivative in space to calculate the density profiles of CO₂ at any point in time.

This appendix first presents the process of discretization of the governing equation used in the FTCS technique. The discretized governing equation is used to

calculate the spatial and temporal distribution of pressure. Two software packages, Maple and Matlab, were independently used to solve the governing equation and its associated boundary conditions using the FTCS technique. Therefore this appendix also presents their respective software codes. For the software code related to Maple, the executable lines of code are represented in a block. The remaining lines of text are descriptive and are not executed by the software. For the software package Matlab, all the associated lines of code presented in the appendix are executed by the software except for the text in any given line that is preceded by the symbol %.

A.2 DISCRETIZATION PROCEDURE

In the software package Maple, the governing equation was given as an input in the form of a partial differential equation and no discretization was separately performed in the input code, although the technique to be used (i.e. the FTCS technique) for solving the partial differential equation was specified. For Matlab, the discretized governing equation was given as the input code, unlike in Maple. Although both software packages used the FTCS technique for solving the governing equation, the method of input for them was completely different, which will be presented later.

As described in Chapter 3, the governing equation that describes the flow of supercritical CO₂ in a porous medium is

$$\varepsilon_v \frac{\partial \rho}{\partial t} = \frac{\partial \left(\rho \frac{\kappa}{\mu} \frac{\partial P}{\partial x} \right)}{\partial x} \quad (\text{A-1})$$

Nomenclature of the variables used in this appendix is the same as in Chapter 3. For simplifying the calculations, Eq. A-1 uses ρ as the dependent variable. Since the governing equation describes a process operating over a range of pressures, the viscosity of CO₂ is not a constant. Changes in viscosity are therefore incorporated into Eq. A-1 by the empirical relation as

$$\mu(\rho) = a^* \rho^2 + b^* \rho + c^* \quad (\text{A-2})$$

where a^* , b^* and c^* are constants. Combining Eq. A-2 with Eq. A-1 and using the general cubic equation of state to express P in terms of ρ , we get

$$\varepsilon_v \frac{\partial \rho}{\partial t} = \left(\frac{\kappa}{\mu} \left(\frac{\partial \rho}{\partial x} \right)^2 \left(\frac{f'(\rho)}{\mu(\rho)} - \frac{\rho}{(\mu(\rho))^2} \mu'(\rho) f'(\rho) + \frac{\rho}{\mu(\rho)} f''(\rho) \right) + \frac{\rho f'(\rho)}{\mu(\rho)} \frac{\partial^2 \rho}{\partial x^2} \right) \quad (\text{A-3})$$

where the expressions for $\mu'(\rho)$, $f'(\rho)$ and $f''(\rho)$ are given by

$$\mu'(\rho) = 2a^* \rho + b^* \quad (\text{A-4a})$$

$$\begin{aligned} f'(\rho) &= \frac{RT}{1-\rho b} + \frac{\rho b RT}{(1-\rho b)^2} - \frac{2a\rho}{(1+\rho\sigma b)^2(1+\rho\epsilon b)} + \frac{\rho^2 a}{(1+\rho\sigma b)^2(1+\rho\epsilon b)^2} (b(\sigma + \epsilon) + 2b^2 \rho\sigma\epsilon) \end{aligned} \quad (\text{A-4b})$$

$$\begin{aligned} f''(\rho) &= \frac{2bRT}{(1-\rho b)^2} + \frac{2\rho b^2 RT}{(1-\rho b)^3} - \frac{2a}{(1+\rho\sigma b)(1+\rho\epsilon b)} + \frac{2a\rho}{(1+\rho\sigma b)^2(1+\rho\epsilon b)^2} (b(\sigma + \epsilon) + 2b^2 \rho\sigma\epsilon) \\ &+ (b(\sigma + \epsilon) + 2b^2 \rho\sigma\epsilon) \times \left(\frac{4a\rho}{(1+\rho\sigma b)^2(1+\rho\epsilon b)^2} - \frac{2a\rho^2 \epsilon b}{(1+\rho\sigma b)^2(1+\rho\epsilon b)^3} - \frac{2a\rho^2 \sigma b}{(1+\rho\sigma b)^3(1+\rho\epsilon b)^2} \right) \\ &+ \frac{2a\rho^2 b^2 \sigma\epsilon}{(1+\rho\sigma b)^2(1+\rho\epsilon b)^2} \end{aligned} \quad (\text{A-4c})$$

Equations A-2 – A-4 are solved together numerically using the FTCS technique as an explicit method. The FTCS technique uses a forward derivative in time and central derivative in space to calculate future values of the density of CO₂. Equation A-3 consists of partial derivatives of ρ in t and x . The time and space derivatives in Eq. A-3 are discretized as

$$\frac{\partial \rho}{\partial t} = \frac{\rho(x_i, t_n + \tau) - \rho(x_i, t_n)}{\tau} \quad (\text{A-5})$$

$$\frac{\partial^2 \rho}{\partial x^2} = \frac{\rho(x_i + h, t_n) + \rho(x_i - h, t_n) - 2\rho(x_i, t_n)}{h^2} \quad (\text{A-6})$$

where $\rho(x_i, t_n)$ is the density of CO₂ in the MLC at $x_i = (i-1)h - L/2$ and $t_n = (n-1)\tau$. As illustrated in Figure A-1, h is the grid spacing in x and τ is the grid spacing in t . Furthermore i ($i \geq 1$) and n ($n \geq 1$) denote the step number in space and time, respectively. For nomenclature, we introduce the shorthand

$$\rho_i^n = \rho(x_i, t_n) \quad (\text{A-7})$$

Using Eqs. A-5 to A-7, Eq. A- 3 can now be rewritten as

$$\begin{aligned} \varepsilon_v \left(\frac{\rho_i^{n+1} - \rho_i^n}{\tau} \right) = & \kappa \left(\frac{\rho_{i-1}^n - \rho_i^n}{h} \right)^2 \left(\frac{f'(\rho_i^n)}{\mu(\rho_i^n)} - \frac{\rho_i^n \times \mu'(\rho_i^n) \times f'(\rho_i^n)}{(\mu(\rho_i^n))^2} + \frac{\rho_i^n f''(\rho_i^n)}{\mu(\rho_i^n)} \right) \\ & + \frac{\rho_i^n f'(\rho_i^n)}{\mu(\rho_i^n)} \left(\frac{\rho_{i+1}^n + \rho_{i-1}^n - 2\rho_i^n}{h^2} \right) \quad (\text{A-8}) \end{aligned}$$

which, on rearranging, can be used to calculate the future value of density ρ_i^{n+1} using its current value ρ_i^n . Since we know the initial condition, i.e., the value of the grid points corresponding to $n = 1$, the values of the grid points at $n = 2$ can be calculated from Eq. A-8. Similarly, values of the grid points at $n = 3$ are calculated using those at $n = 2$. Progressing in this manner the FTCS technique can be used to calculate the solution to any partial differential equation by calculating the value of the interior grid points.

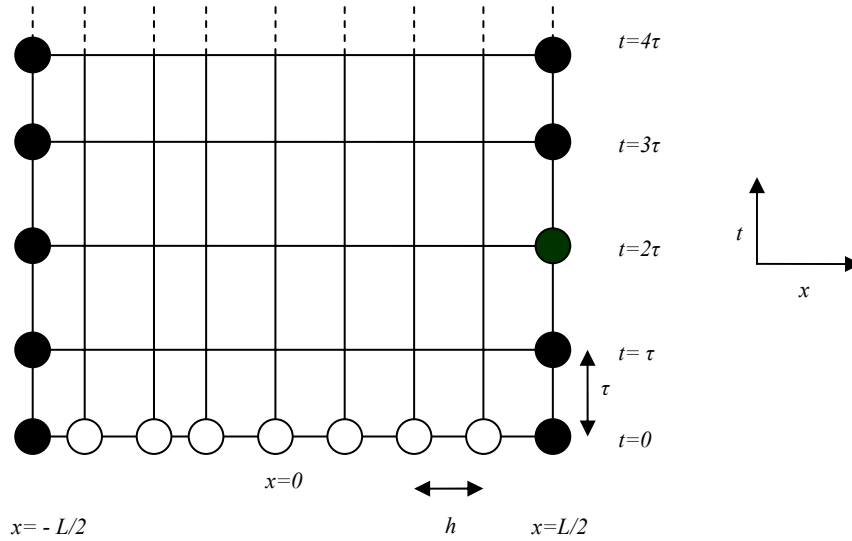


Figure A-1: Schematic representation of a discretized problem with initial value (empty circles) and boundary values (filled circles) specified. The solution is divided into a two dimensional grid with axes x and t . The grid spacing of x is h and the grid spacing of t is τ .

A.3 MAPLE CODE FOR THE CALCULATION OF DISTRIBUTION OF PRESSURE

Dependent variable used: $u(x,t)$ which represents density as a function of space (x) and time (t)

Independent variables used: x and t

INITIALIZING ALL VARIABLES USED IN CALCULATION OF DENSITY OF CO₂ AS A FUNCTION OF x AND t

```
>
L := 0.02: Sample dimensions in meters
εv := 0.15: Sample porosity (-)
κ := 1·10-17: Permeability of the sample in m2
μ := 1.7·10-13·u(x,t)2 + 8.2·10-11·u(x,t) + 1.8·10-5: Viscosity of Carbon Dioxide in Pa s
R := 8.314: Gas Constant in J/mol/K
T := 363.15: Temperature of vessel in K
ρ0 := 18050: Initial density of CO2 at 90°C and 40 MPa pressure in mol/m3
ρend := 35: Density of CO2 at 90°C and 0.1 MPa pressure in mol/m3
tdp := 12·60: Depressurization time in seconds
>
Peng Robinson EOS Constants:- (All correspond to SI Units)
a := 0.2773:
ε := 2.414:
σ := -0.414
b := 2.668·10-5:
```

INITIALIZATION OF THE GOVERNING PARTIAL DIFFERENTIAL EQUATION AND ASSIGNMENT OF THE VARIABLE PDE TO THE GOVERNING EQUATION

$$PDE := \epsilon v \cdot \text{diff}(u(x, t), t) = \kappa \cdot \text{diff} \left(\left(\frac{u(x, t)}{\mu} \cdot \text{diff} \left(\left(\frac{R \cdot T}{\left(\frac{1}{u(x, t)} - b \right)} - \frac{a}{\left(\frac{1}{u(x, t)} + \epsilon \cdot b \right) \cdot \left(\frac{1}{u(x, t)} + \sigma \cdot b \right)} \right), x \right) \right), x \right) :$$

ASSIGNMENT OF THE VARIABLE *IBC* TO THE INITIAL AND BOUNDARY CONDITIONS

$$IBC := \left\{ u(x, 0) = \rho_0, u\left(-\frac{L}{2}, t\right) = \rho_0 - \frac{\rho_0 - \rho_{end}}{tdp} \cdot t, u\left(\frac{L}{2}, t\right) = \rho_0 - \frac{\rho_0 - \rho_{end}}{tdp} \cdot t \right\} :$$

SOLVING THE PARTIAL DIFFERENTIAL NUMERICALLY AND DEFINING THE METHOD USED WITH RELEVANT TIME STEP, THE DATA FOR WHICH ARE STORED IN THE VARIABLE *pds*

$$pds := pdsolve\left(PDE, IBC, numeric, time = t, range = -\frac{L}{2} .. \frac{L}{2}, method = ForwardTimeCenteredSpace, timestep = \frac{1}{100000}\right) :$$

ASSIGNMENT OF A STORAGE VARIABLE *densityxt* FOR STORING VALUES OF DENSITY FOR EVERY x and t

$$densityxt := pds:-value() : densityxt(0, 12) :$$

>

A.4 MATLAB CODE FOR THE CALCULATION OF DISTRIBUTION OF PRESSURE

```
%Declaration of Variables

%%Sample Characteristics

L=0.02;                %Length of the sample in m
epsv=0.15;             %Sample Porosity (-)
k=1E-17;               %Sample permeability in m^2
%%Peng Robinson EOS Constants (SI Units)
a=0.2776;
b=2.668E-05;
eps=1-sqrt(2);
sig=1+sqrt(2);
%%Extraction Condition related variables
rho_0=18050;           %density of SC CO2 in mol/m3
rho_end=35;
finaltime=12*60;       %Final value of time in s
alpha=(rho_0-rho_end)/finaltime;
                        %Rate of change of CO2 density during
                        %linear depressurization
T=363.15;              %Temperature in K
R=8.314;               % Gas constant in J/mol/K
%%FTCS technique related variables
N=51;                  %Number of steps in space (-)

h=L/(N-1);             %step size in space (m)
rho=[-L/2:h:L/2];      %Fixing the horizontal matrix (1xN)
                        %that will store values of density for a given time,
                        %for every step in space (from 1 to N)

rho(1,:)=rho_0;        %Defining initial density in the grid at t=0.

nmax=100000;           %Number of steps in time (-)

tau=finaltime/nmax;    %Step size in time (s)

%%Empirical Viscosity constants

astar=1.7E-13;
bstar=8.2E-11;
cstar=1.8E-05;

X=[-L/2:h:L/2]; %Space axis (used for plotting)

for n=1:1:nmax          %A ROW (time axis) IS DESIGNATED BY "n".
                        %"n" is the row number
    t=(n)*tau;          %time at a given step number
    rho(n+1,1)=rho_0-alpha*t; %Value of left boundary
    rho(n+1,N)=rho_0-alpha*t; %Value of right boundary

%Now that we have traversed a numerical value of "t" in time, we
calculate all the values of "rho" corresponding to this "t" at all "x"
```

```

for ii=2:1:N-1
    %A COLUMN IS DESIGNATED BY "ii".
    %Hence "ii" is the column number

    %Discretized governing equation which is described in Eq. A-8
    % with f1 (f'(rho)), f2 (f''(rho)) and f3(viscosity(rho))

    f1=R*T/(1-rho(n,ii)*b) + rho(n,ii)*b*R*T/(1-rho(n,ii)*b)^2
    -
    2*a*rho(n,ii)/(1+rho(n,ii)*eps*b)/(1+rho(n,ii)*sig*b)+rho(n,ii)*r
    ho(n,ii)*a*(b*(sig+eps)+(2*b^2*eps*sig*rho(n,ii)))/(1+rho(n,ii)*e
    ps*b)^2/(1+rho(n,ii)*sig*b)^2;

    f2=2*b*R*T/(1-rho(n,ii)*b)^2 + 2*rho(n,ii)*b^2*R*T/(1-
    rho(n,ii)*b)^3 - 2*a/(1+rho(n,ii)*eps*b)/(1+rho(n,ii)*sig*b)
    +
    2*a*rho(n,ii)*(b*(sig+eps)+2*b^2*eps*sig*rho(n,ii))/(1+rho(n,ii)*
    eps*b)^2/(1+rho(n,ii)*sig*b)^2+(4*a*rho(n,ii)/(1+rho(n,ii)*eps*b)
    ^2/(1+rho(n,ii)*sig*b)^2 -
    2*rho(n,ii)*rho(n,ii)*a*eps*b/(1+rho(n,ii)*eps*b)^3/(1+rho(n,ii)*
    sig*b)^2 -
    2*rho(n,ii)*rho(n,ii)*a*sig*b/(1+rho(n,ii)*eps*b)^2/(1+rho(n,ii)*
    sig*b)^3 ) *(b*(eps+sig) + 2*rho(n,ii)*sig*eps*b^2)+
    rho(n,ii)*rho(n,ii)*a*(2*b^2*sig*eps)/(1+rho(n,ii)*eps*b)^2/(1+rh
    o(n,ii)*sig*b)^2;

    f3=2*astar*rho(n,ii)+bstar;

    %Now that f1 (f'(rho)), f2 (f''(rho)) and f3(meu(rho))
    %have been calculated, we can calculate the
    %future value of density once we know the viscosity at
    %this point of time "t"

    %Viscosity function calculation

    meu=astar*(rho(n,ii))^2+bstar*rho(n,ii)+cstar;

    %Density calculation
    rho(n+1,ii)=rho(n,ii)+(k *tau/epsv)*( ((rho(n,ii+1)-
    rho(n,ii))/h)^2 * (f1/meu-(rho(n,ii)/(meu)^2)*f3*f1 +
    (rho(n,ii)/meu)*f2)+
    (rho(n,ii+1)+rho(n,ii-1)-2*rho(n,ii))/(h^2)*rho(n,ii)/meu*f1);
    end
end

```

A.5 SIMULATION RESULTS OF MAPLE AND MATLAB

Figure A-2 shows the results of temporal and spatial distribution of pressure within the green body during depressurization lasting 0.2 h (Figure A-2a) and 6 seconds (Figure A-2b) from supercritical extraction conditions at 90°C and 40 MPa. The values of parameters used for the simulation by both software codes are given in Table A-1. The output data for Maple and Matlab were the density values of CO₂, which were used to manually calculate pressure of CO₂ using the Peng-Robinson equation of state. The symbols represent the Maple data and the lines represent the Matlab data. Figure A-2 shows that both the software packages agree to the same values for a given set of experimental conditions.

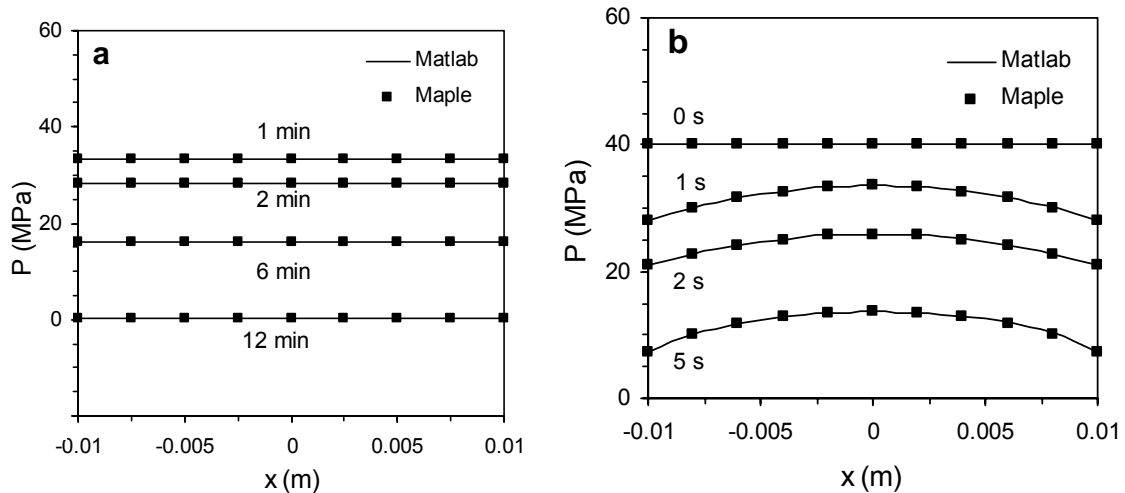


Figure A-2: Distribution of pressure in the green body during depressurization lasting a) 0.2 h (12 min) and b) 6 seconds, from conditions of 90°C and 40 MPa. The symbols indicate simulation values of Maple and lines indicate simulation values of Matlab.

The Maple software was given input in the form of an un-discretized governing equation with non-homogeneous boundary conditions, although it was also commanded to use the FTCS technique. For Matlab, the governing equation input was given in a

discretized form as shown in Eq. A-8. Since both software packages converged to the same solution using the same technique, the FTCS technique, along with the discretization procedure, was confirmed.

Table A-1: Summary of values used for simulation of Figure A-2.

Parameters (Units)	Values	
	Fig. A-2a	Fig. A-2b
$\kappa \text{ (m}^2\text{)}$	1×10^{-17}	1×10^{-17}
$L \text{ (m)}$	0.02	0.02
$\varepsilon_v \text{ (-)}$	0.15	0.15
$t^{DP} \text{ (s or h)}$	0.2 h	6 s
$P^o \text{ (MPa)}$	40	40
$T \text{ (}^\circ\text{C)}$	90	90

A.6 REFERENCES

1. A. Fenghour, W.A. Wakeham and V. Vesovic, "The Viscosity of Carbon Dioxide," *J. Phys. Chem. Ref. Data*, **27** [1] 31-44 (1998).
2. J. M. Smith, H. C. Van Ness and M. M. Abbott, *Introduction to Chemical Engineering Thermodynamics*, 6th Ed., McGraw Hill, New York, 2001.
3. D.-Y. Peng and D. B. Robinson, "A New Two-Constant Equation of State" *Ind. Eng. Chem. Fundam.*, **15** [1] 59-64 (1976).
4. A. L. Garcia, *Numerical Methods for Physics*, 2nd Ed, Prentice Hall, New Jersey, 2000.

VITA

Kumar Krishnamurthy was born in Mumbai (Bombay), India on August 7th, 1984. He commenced his Bachelor of Engineering Degree in Chemical Engineering from University of Mumbai, India in August 2002 and completed it in June 2006 with a First Class Degree in Chemical Engineering.

Kumar Krishnamurthy was accepted in University of Missouri – Columbia on March 1st, 2006 and began his graduate studies in August 21st, 2006. Upon approval of this thesis, Kumar will have completed the requirements for Master of Science Degree in Chemical Engineering with the granting of the degree in July 2008. On 1st September, 2008, he will commence his job as a Research Engineer in Continental AG at Hannover, Germany.